

Non-hermitian topology and entanglement in an optomechanical superlattice

Wojciech Brzezicki,^{1,2} Timo Hyart,^{3,4} and Francesco Massel⁵

¹*Institute of Theoretical Physics, Jagiellonian University,
ulica S. Łojasiewicza 11, PL-30348 Kraków, Poland*

²*International Research Centre MagTop, Institute of Physics,
Polish Academy of Sciences, Aleja Lotników 32/46, PL-02668 Warsaw, Poland*

³*Computational Physics Laboratory, Physics Unit,
Faculty of Engineering and Natural Sciences, Tampere University, FI-33014 Tampere, Finland*

⁴*Department of Applied Physics, Aalto University, 00076 Aalto, Espoo, Finland*

⁵*Department of Science and Industry Systems, University of South-Eastern Norway, PO Box 235, Kongsberg, Norway*

The interplay between topology, dissipation and nonlinearities can give rise to a wealth of new phenomena and pave the way for novel topological lasers, sensors and other quantum devices. Along these lines, we propose here an optomechanical setup in which the concomitant presence of a spatially modulated external drive and dissipation gives rise to a topologically nontrivial state for mechanical and optical excitations. We are able to show that the one-dimensional system considered here exhibits topologically protected end states for which mechanical and optical degrees of freedom are entangled. We show such entanglement to be robust with respect to the presence of nonzero-temperature baths and we propose a protocol for experimental observation of the entanglement.

Introduction. Since the seminal work by Thouless, Kohomoto, Nightingale and den Nijs [1], describing the quantization of the Hall conductance in terms of topological invariant of their Hamiltonian, topology has played a central role in the determination of properties of condensed matter systems. The classification of Hamiltonians belonging to Altland-Zirnbauer symmetry classes [2], characterized by particle-hole, time reversal and chiral symmetries, has led to the systematic understanding of the relationship between topological invariants and symmetries in various dimensional systems – the tenfold way [3–5]. Over the years, it has been realized that the role of topology in determining the properties of physical systems extends beyond the realm of solid-state electron systems, with ramifications, for instance, into the physics of optical and optomechanical systems [6–29], where the combination of topological and non-hermitian physics has recently led to the realization of topological lasers [10] and topologically protected entangled states [11, 12]. Upon broadening the scope of the topological considerations to include the non-hermitian effects present in open systems [30], it was discovered that the generalization of the topological classification to non-Hermitian systems implies an extension of the tenfold way to 38 symmetry classes [31].

In the present work, we propose a new approach to topology in optomechanical system, investigating the role of spatially-modulated drive and dissipation in determining the topological properties of an optomechanical chain, taking into account the role played by quantum fluctuations. We show that an external drive can induce a topologically nontrivial phase, leading, for open boundary conditions, to topologically protected end states. Importantly, when the system is in the topologically nontrivial phase we obtain robust stationary-state entanglement between the mechanical and optical end modes.

The generation of entanglement between optical and mechanical modes in optomechanical systems has been experimentally demonstrated in a pulsed regime [32], but earlier theoretical proposals [33] of stationary-state entanglement require the system to be in the so-called ultrastrong coupling regime, which is difficult to achieve experimentally (see [34] for a relatively recent demonstration of an optomechanical system in the ultrastrong coupling regime). Conversely, in our system, for realistic experimental parameters, we can achieve stationary-state entanglement that survives in the presence of significant thermal noise for the mechanical degrees of freedom, and tolerates moderate amounts of optical noise. Furthermore, since the end states are topologically protected, our results are expected to remain valid also in the presence of significant disorder in all model parameters describing the optical cavity modes and mechanical oscillators of the optomechanical chain. Finally, our analysis suggests that, beyond the instability threshold for end modes, topological lasing of entangled optomechanical modes is possible.

The system. Our setup is constituted by a one-dimensional lattice of conventional optomechanical cavities, each of which is driven by a strong coherent tone. On each site, we choose to detune the drive from the optical cavity resonance by an amount corresponding to the mechanical resonant frequency ω_m . The detuning can either be negative ($\omega_R = \omega_c - \omega_m$, red-detuned drive) or positive ($\omega_B = \omega_c + \omega_m$, blue-detuned drive). Echoing the analysis performed in Ref. [35, 36], where the properties of a non-hermitian one-dimensional chain were modulated in a dissipative superlattice pattern according to a ABBA pattern, we choose to alternate the drive of the optomechanical chain in a blue-red-red-blue (BRRB) driving pattern (see Fig. 1). Our choice reflects the idea that, within the framework of linear op-

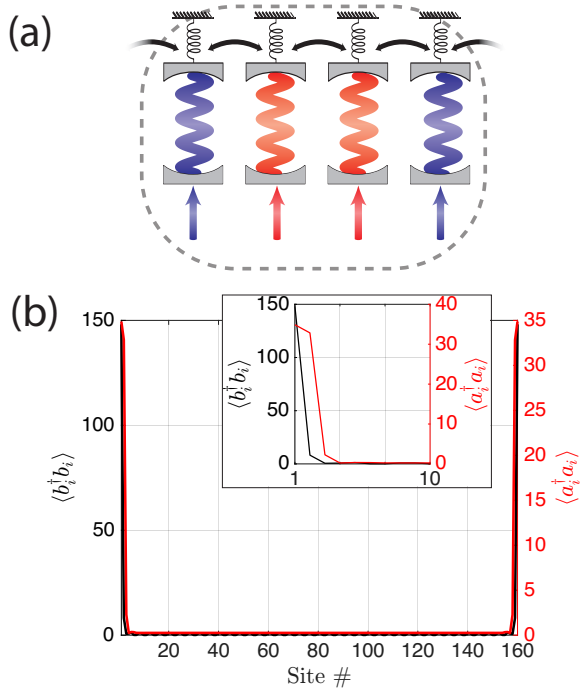


Figure 1. (a) Cartoon depiction of the superlattice unit cell. Each optomechanical system is driven either on the blue (G_+ , first and fourth sites) or the red (G_- , second and third) mechanical sideband. The coupling between sites arises from a hopping term (J) between the mechanical modes. (b) Mechanical (black) and optical (red) equilibrium population of the chain for $G_+ = 0.242$, $G_- = 1$, $J = 0.5$, $\gamma = 10^{-4}$, and $n_c = n_m = 0$. For this value of G_+ the system is approaching the instability for the end states. Energies are in units of κ .

tomechanics [37, 38], in the presence of a strong driving coherent tone, an optical cavity coupled through radiation pressure to a mechanical oscillator can be analyzed in terms of two linearly-coupled harmonic oscillators describing the dynamics of the electromagnetic field and mechanical fluctuations. In the so-called sideband-resolved regime, a drive at a frequency ω_B will induce an effective parametric-down-converter ($a^\dagger b^\dagger + \text{h.c.}$) coupling between electromagnetic (a) and mechanical (b) degrees of freedom, while a drive at ω_R will lead to a coherent beam-splitter process ($a^\dagger b + \text{h.c.}$) between mechanical and electromagnetic fluctuations. For an isolated optomechanical system, a beam-splitter coupling can lead to ground state cooling of the mechanical mode [39, 40], while the former implies amplification and, ultimately, instability and lasing of the mechanical motion [41, 42]. These two effects can be understood in terms of an effective increase (respectively, decrease) of the mechanical damping rate.

In addition to the on-site coherent drives, we also introduce a hopping term between mechanical excitations, which can be realized, for instance, in an optomechanical

crystal [43] combining, in a single structure, the properties of photonic [44, 45] and phononic [46, 47] crystals. Combining these elements, the Hamiltonian describing the coherent part of the dynamics for the mechanical and optical fluctuations in a chain comprising $4N$ sites is given by

$$H = \sum_{j=0}^{N-1} [G_+(a_{4j+1}^\dagger b_{4j+1}^\dagger + a_{4j+4}^\dagger b_{4j+4}^\dagger) + G_-(a_{4j+2}^\dagger b_{4j+2}^\dagger + a_{4j+3}^\dagger b_{4j+3}^\dagger)] - J \sum_{j=1}^{4N-1} b_j^\dagger b_{j+1} + \text{h.c.}, \quad (1)$$

where the coupling constant G_+ (G_-) models the parametric down conversion (coherent exchange) process induced by a coherent blue-sideband (red-sideband) drive, and J describes the hopping amplitude between the mechanical modes b_j and a_i are the lowering operator associated with the electromagnetic modes (see [48] for more details).

In addition to the unitary dynamics described by Eq. (1), we model the coupling of each site i to the environment introducing the (noise) input operators $a_{\text{in},i}$ and $b_{\text{in},i}$ with expectation values $\langle a_{\text{in},i}(t) a_{\text{in},i}^\dagger(t') \rangle = (n_c + 1) \delta(t - t')$ and $\langle b_{\text{in},i}(t) b_{\text{in},i}^\dagger(t') \rangle = (n_m + 1) \delta(t - t')$, respectively, where the system-environment coupling rates for optical and mechanical modes are given by κ and γ respectively. We note that, while the thermal occupation for the optical bath n_c can be set to zero, especially for the infrared and the visible-light case, it is not possible to neglect the thermal population of the mechanical bath n_m . The symmetry between the mechanical and optical excitations in Eq. (1) would only allow to replace the hopping of phonons with hopping of photons [49] at zero temperature. We find that a finite value of n_m has detrimental effects on the entanglement properties of the photonic implementation, and therefore, along the lines of Ref. [50], we focus here on the phononic hopping, which, as discussed below, allows for an effective cooling of the mechanical end modes. Nevertheless, while it is necessary to assume that the hopping term is predominant for the ‘‘hot’’ (mechanical) degrees of freedom, we have checked that our results are robust upon inclusion of a small hopping-disorder term for the ‘‘cold’’ (optical) degrees of freedom.

Results. Through a standard approach [48], the dynamics of the system’s degrees of freedom can be solved to give

$$\mathbf{a} = \exp[-i\mathcal{H}_{\text{NH}}t] \mathbf{a}_0 + \int_0^t \exp[-i\mathcal{H}_{\text{NH}}(t - \tau)] \sqrt{\eta} \mathbf{a}_{\text{in}} d\tau \quad (2)$$

where $\mathbf{a} = [a_1, b_1, \dots, a_{4N}, b_{4N}; a_1^\dagger, b_1^\dagger, \dots, a_{4N}^\dagger, b_{4N}^\dagger]^T$ and an analogous definition holds for \mathbf{a}_{in} .

In Eq. (2), $-i\mathcal{H}_{\text{NH}} = -i(\bar{\sigma}_z \mathcal{H} - i\bar{\eta}/2)$ –where \mathcal{H} is the BdG Hamiltonian associated with the Hamiltonian

H given in Eq. (1), $\bar{\sigma}_z = \text{diag}(1, \dots, 1; -1, \dots, -1)$ and $\bar{\eta} = \text{diag}(\kappa, \gamma, \dots; \kappa, \gamma, \dots, \kappa, \gamma)$ can be interpreted as the Jacobian matrix for the quantum dynamical system whose solution is given by Eq. (2). As a consequence, from the dynamical systems perspective, the spectrum of \mathcal{H}_{NH} characterizes the stability of the system. If $E_i = \text{eig}(\mathcal{H}_{\text{NH}})$, the system is stable for $\text{Im} E_i < 0$ only. This is confirmed by the third quantization analysis [51] of the dynamics of our system [48].

Crucial insight into the properties of the system, can be obtained exploring the topological properties of the Hamiltonian \mathcal{H}_{NH} . To this end we can define the effective Hermitian Hamiltonian $\mathcal{H}_{\text{eff}}(\eta, k) = \eta S - iS\mathcal{H}_{\text{NH}}(k)$, where $\mathcal{H}_{\text{NH}}(k)$ is the k-space BdG Hamiltonian and $S = \frac{1}{2}\sigma_0 \otimes [\sigma_z \otimes \sigma_0 \otimes (\sigma_z + \sigma_0) + \sigma_0 \otimes \sigma_z \otimes (\sigma_0 - \sigma_z)]$ encodes the symmetry properties of $\mathcal{H}_{\text{NH}}(k)$ (see Ref. [36, 48]). In general, it is possible to prove [35] that a nontrivial Chern number associated with \mathcal{H}_{eff} , determines the nontrivial topology for the corresponding non-hermitian Hamiltonian \mathcal{H}_{NH} and therefore the appearance of topologically protected end states. For the optomechanical chain under consideration, we have $C = 4$ indicating that there are 4 topologically protected end states with $\text{Re} E = 0$ at each end of the chain [48].

In Fig. 2 we have depicted a phase diagram for \mathcal{H}_{NH} as a function of G_- and G_+ , characterizing the properties of the imaginary parts of the end and bulk state energies $\text{Im} E_e$ and $\text{Im} E_b$. On the $G_- = 1$ line, we have that, for small G_+ , $\text{Im} E_e$ lies within the $\text{Im} E_b$ band (panel (a)). Increasing G_+ leads to the appearance of a finite gap between $\text{Im} E_e$ and the $\text{Im} E_b$ band (panel (b)). Upon further increase of G_+ we observe a transition to a situation where, at first, $\text{Im} E_e > 0$ and $\text{Im} E_b < 0$ (panel (c)) and eventually, $\text{Im} E_{e,b} > 0$ (panels (d,e)). While the situation depicted in panel (d) is characterized by a band crossing the $\text{Im} E = 0$ line, in panel (e) a gap in the bulk spectrum appears. A cross section of the phase diagram across the points (a-d) in Fig. 2, depicting the evolution of the spectrum as a function of G_+ is depicted in Fig. 3. The case $\text{Im} E_{e,b} < 0$, $\text{Im} E_e \rightarrow 0^-$, leads to an increase in the population of the end states in stationary conditions, and to its divergence when $\text{Im} E_e > 0$ (while $\text{Im} E_b < 0$).

As anticipated, the nature of the end states is best captured considering the equilibrium properties of the chain when coupled to a thermal bath. Given that we are considering Gaussian states and a linear dynamics, the properties of the system are entirely captured by its covariance matrix

$$V_{\bar{a}, \bar{a}^\dagger} = \begin{bmatrix} \langle a_1 a_1^\dagger \rangle & \langle a_1 b_1^\dagger \rangle & \langle a_1 a_1 \rangle & \langle a_1 b_1 \rangle & \dots \\ \langle b_1 a_1^\dagger \rangle & \ddots & & & \\ \vdots & & & & \end{bmatrix}, \quad (3)$$

which can be evaluated in equilibrium conditions, through the solution of the stationary-state Lyapunov

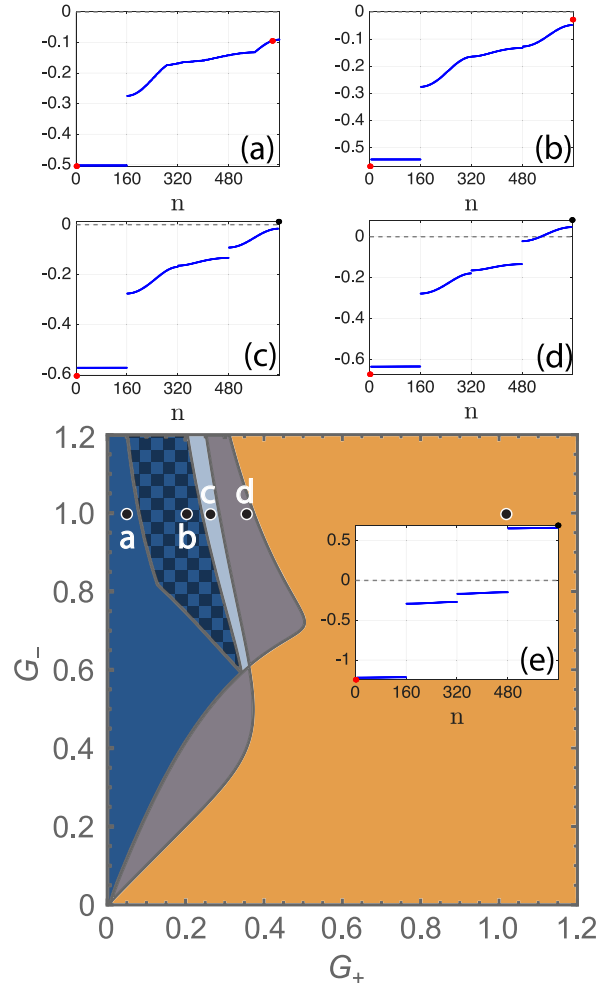


Figure 2. Phase diagram of \mathcal{H}_{NH} in the (G_-, G_+) plane. (a-e) Imaginary part of the spectrum ($\text{Im} E$) for the different values of (G_+, G_-) indicated in the main panel. All other parameters as in Fig. 1. Blue lines: $\text{Im} E_b$, red dots: $\text{Im} E_e$ (< 0), black dots: $\text{Im} E_e$ (> 0)

equation for $V_{\bar{a}, \bar{a}^\dagger}$

$$\mathcal{H}_{\text{NH}} V_{\bar{a}, \bar{a}^\dagger} - V_{\bar{a}, \bar{a}^\dagger} \mathcal{H}_{\text{NH}}^\dagger = -iD \quad (4)$$

with $D = [\kappa(n_a + 1), \gamma(n_b + 1), \kappa n_a, \gamma n_b, \dots]$. As discussed in [48], the expression for D can be derived both from a dynamical systems and a third quantization perspective. As expected, keeping all other parameters fixed, for G_+ approaching the instability transition $\text{Im} E_e \rightarrow 0^-$ (but $\text{Im} E_b < 0$), the end populations of mechanical and optical modes diverge. This is reminiscent of what happens for a single optomechanical system driven on the blue sideband, and therefore suggests the possibility of optomechanical lasing for the topologically protected end states. Although the full description of the lasing ([52, 53]) falls beyond the linearized model employed here, the dynamics of the end states is well captured by

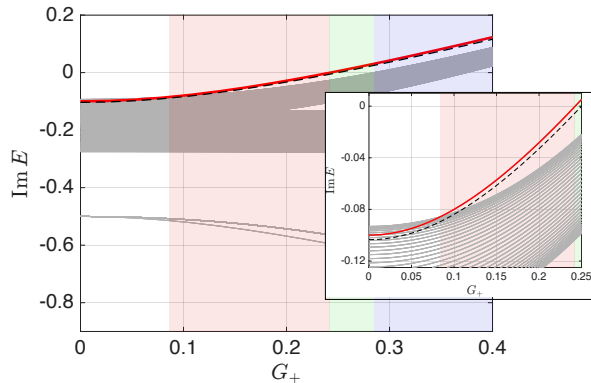


Figure 3. Imaginary part of the spectrum for the OBC chain, same parameters as in Fig. 1. The red line denotes $\text{Im } E_e$, the pink stripe the region for which $\text{Im } E_b < \text{Im } E_e < 0$ (stable end and bulk states), the green one the region $\text{Im } E_b < 0 < \text{Im } E_e$ (unstable end, stable bulk), and the blue one $0 < \text{Im } E_b < \text{Im } E_e$ (unstable end and bulk). The black line denotes the largest value of $\text{Im } E_e$ for the two-site problem [48].

a localized description of the end modes in terms of a two-sites linearized effective model, so that the physics of our system for $\text{Im } E_e > 0$ and $\text{Im } E_b < 0$ will be equivalent to the one controlling optomechanical cavities in the optomechanical lasing regime [54–56].

In addition to the local population, through a standard analysis [57], we can explore the entanglement properties of the chain, evaluating the negativity E_N between two modes [48]. Of particular interest is that, at zero temperature, irrespective of the strength of the drives, optical and mechanical modes pertaining to the first site are entangled (see [48] for a full characterization of the entanglement properties within a superlattice cell).

For the single cavity in the presence of a blue-sideband drive, while, in principle, it is possible to have stationary entanglement [33], its value is severely limited by stability constraints, which, in the rotating-wave approximation can be expressed by the condition $G_+ < \sqrt{\gamma\kappa}/2$. As a consequence, optomechanical entanglement for a single optomechanical cavity has been predicted either far from the sideband-resolved regime or for a pulsed drive [33, 58, 59] only. Owing to the demanding parameter regime required in the former case, experimental verification has been provided in the latter case only [32].

For the setup described here, we can show that significant entanglement between optical and mechanical degrees of freedom survives within the topologically protected end state, even beyond the single-site instability threshold (see Fig. 4). The stability and entanglement properties of the end state can be understood in terms of an effective bath induced by the chain: mechanical excitations can hop from the end sites of the chain (driven on the blue sideband) towards the interior of the chain. The

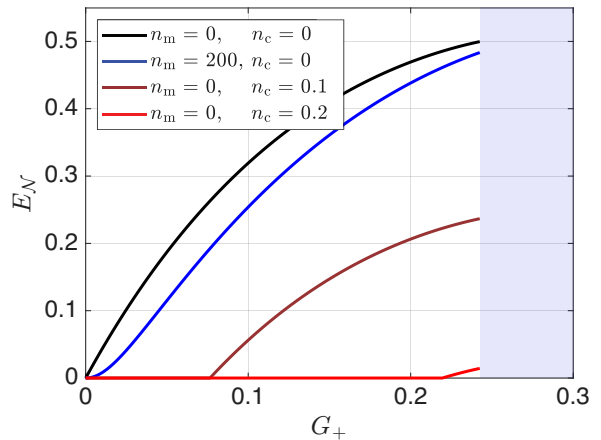


Figure 4. Negativity E_N measuring the entanglement between optical and mechanical modes within the first site (a_1 and b_1) as a function of G_+ for different values of the mechanical bath population. The entanglement is not strongly affected by a thermal population of the mechanical bath.

red-detuned drive G_- on the sites next to the end leads to the cooling of the mechanical excitations to the (near-zero) effective temperature of the optical bath. This process is well captured by a two-site model, describing the G_+ -dependence of the end-states dissipation properties [48]. More specifically, in the limit of vanishing blue-sideband drive $G_+ \rightarrow 0$, we have

$$\text{Im } E_{2\text{-site}} = -\frac{\gamma}{2} - (\kappa - \gamma) \frac{J^2}{G_-^2} \left(1 - \frac{J^2}{G_-^2}\right) + O(J/G_-)^5 \quad (5)$$

while for $G_+ \rightarrow \infty$ we have

$$\text{Im } E_{2\text{-site}} \simeq -\frac{\kappa + \gamma}{2} + \sqrt{\frac{(\kappa - \gamma)^2}{4} + 4G_+^2}. \quad (6)$$

Importantly, for typical experimental parameters, entanglement is robust with respect to a finite (even large) thermal population of the mechanical bath (see Fig. 4). This is in agreement with what is predicted for single optomechanical systems driven on the red sideband away from the sideband-resolved regime [48].

The topological character of the end states is apparent when considering experimental imperfections that might lead to random offsets in the on-site frequencies for mechanical and optical modes and to the appearance of a random hopping for the optical degrees of freedom. We have verified that adding disorder for the hopping (for mechanical and optical modes) and on-site potential, does not alter the picture outlined here [48]. This aspect is particularly relevant when discussing the experimental observability of optomechanical entanglement. Analogously to what was suggested in the case of a single optomechanical system [60], we envisage the measurement of the mechanical spectrum through the coupling to a

probe cavity driven on the red sideband, whose spectrum reproduces the mechanical one, which, however, owing to backaction, alters the values of γ and n_m [48].

Conclusions. We have discussed here the properties of a chain of optomechanical systems in the presence of site-dependent optical drives. We have demonstrated that the chain possesses nontrivial topological properties leading to the existence of topologically protected states both for mechanical and optical modes. Furthermore, we have demonstrated that mechanical and optical end states are entangled and that such entanglement is robust with respect to external perturbations, paving the way for entanglement in topological lasers. Our findings provide evidence of a strong quantum property (entanglement) within a non-hermitian topological system.

Acknowledgements. WB acknowledge support by Narodowe Centrum Nauki (NCN, National Science Centre, Poland) Project No. 2019/34/E/ST3/00404 and partial support by the Foundation for Polish Science through the IRA Programme co-financed by EU within SG OP. FM thanks Kjetil Børkje and Mika Sillanpää for fruitful discussion. FM acknowledges financial support from the Research Council of Norway (Grant No. 333937) through participation in the QuantERA ERA-NET Cofund in Quantum Technologies (project MQSens) implemented within the European Union's Horizon 2020 Programme.

-
- [1] D. Thouless, M. Kohmoto, M. Nightingale, and M. d. Nijs, Quantized Hall Conductance in a Two-Dimensional Periodic Potential, *Physical Review Letters* **49**, 405 (1982).
- [2] A. Altland and M. R. Zirnbauer, Nonstandard symmetry classes in mesoscopic normal-superconducting hybrid structures, *Physical Review B* **55**, 1142 (1997).
- [3] A. P. Schnyder, S. Ryu, A. Furusaki, and A. W. W. Ludwig, Classification of topological insulators and superconductors in three spatial dimensions, *Phys. Rev. B* **78**, 195125 (2008).
- [4] A. Kitaev, Periodic table for topological insulators and superconductors, *AIP Conference Proceedings* **1134**, 22 (2009).
- [5] S. Ryu, A. P. Schnyder, A. Furusaki, and A. W. W. Ludwig, Topological insulators and superconductors: tenfold way and dimensional hierarchy, *New Journal of Physics* **12**, 065010 (2010).
- [6] F. D. M. Haldane and S. Raghu, Possible Realization of Directional Optical Waveguides in Photonic Crystals with Broken Time-Reversal Symmetry, *Physical Review Letters* **100**, 013904 (2008).
- [7] S. Raghu and F. D. M. Haldane, Analogs of quantum-Hall-effect edge states in photonic crystals, *Physical Review A* **78**, 033834 (2008).
- [8] H. Xu, D. Mason, L. Jiang, and J. G. E. Harris, Topological energy transfer in an optomechanical system with exceptional points., *Nature* **537**, 80 (2016).
- [9] R. El-Ganainy, K. G. Makris, M. Khajavikhan, Z. H. Musslimani, S. Rotter, and D. N. Christodoulides, Non-Hermitian physics and PT symmetry, *Nature Physics* **14**, 11 (2018).
- [10] M. A. Bandres, S. Wittek, G. Harari, M. Parto, J. Ren, M. Segev, D. N. Christodoulides, and M. Khajavikhan, Topological insulator laser: Experiments, *Science* **359**, 10.1126/science.aar4005 (2018).
- [11] S. Mittal, E. A. Goldschmidt, and M. Hafezi, A topological source of quantum light, *Nature* **561**, 502 (2018).
- [12] A. Blanco-Redondo, B. Bell, D. Oren, B. J. Eggleton, and M. Segev, Topological protection of biphoton states, *Science* **362**, 568 (2018).
- [13] M.-A. Miri and A. Alù, Exceptional points in optics and photonics, *Science* **363**, 10.1126/science.aar7709 (2019).
- [14] T. Ozawa, H. M. Price, A. Amo, N. Goldman, M. Hafezi, L. Lu, M. C. Rechtsman, D. Schuster, J. Simon, O. Zeitlinger, and I. Carusotto, Topological photonics, *Reviews of Modern Physics* **91**, 015006 (2019).
- [15] J. d. Pino, J. J. Slim, and E. Verhagen, Non-Hermitian chiral phononics through optomechanically induced squeezing, *Nature* **606**, 82 (2022).
- [16] Y. S. S. Patil, J. Höller, P. A. Henry, C. Guria, Y. Zhang, L. Jiang, N. Kralj, N. Read, and J. G. E. Harris, Measuring the knot of non-Hermitian degeneracies and non-commuting braids, *Nature* **607**, 271 (2022).
- [17] T. Dai, Y. Ao, J. Mao, Y. Yang, Y. Zheng, C. Zhai, Y. Li, J. Yuan, B. Tang, Z. Li, J. Luo, W. Wang, X. Hu, Q. Gong, and J. Wang, Non-Hermitian topological phase transitions controlled by nonlinearity, *Nature Physics* **20**, 101 (2024).
- [18] C. Guria, Q. Zhong, S. K. Ozdemir, Y. S. S. Patil, R. El-Ganainy, and J. G. E. Harris, Resolving the topology of encircling multiple exceptional points, *Nature Communications* **15**, 1369 (2024).
- [19] A. Metelmann and A. A. Clerk, Nonreciprocal Photon Transmission and Amplification via Reservoir Engineering, *Physical Review X* **5**, 021025 (2015).
- [20] N. R. Bernier, L. D. Tóth, A. Koottandavida, M. A. Ioannou, D. Malz, A. Nunnenkamp, A. K. Feofanov, and T. J. Kippenberg, Nonreciprocal reconfigurable microwave optomechanical circuit, *Nature Communications* **8**, 604 (2017).
- [21] E. Verhagen and A. Alù, Optomechanical nonreciprocity, *Nature Physics* **13**, 922 (2017).
- [22] D. Malz, L. D. Tóth, N. R. Bernier, A. K. Feofanov, T. J. Kippenberg, and A. Nunnenkamp, Quantum-Limited Directional Amplifiers with Optomechanics, *Physical Review Letters* **120**, 023601 (2018).
- [23] A. Youssefi, S. Kono, A. Bancora, M. Chegnizadeh, J. Pan, T. Vovk, and T. J. Kippenberg, Topological lattices realized in superconducting circuit optomechanics, *Nature* **612**, 666 (2022).
- [24] V. Peano, C. Brendel, M. Schmidt, and F. Marquardt, Topological Phases of Sound and Light, *Physical Review X* **5**, 031011 (2015).
- [25] C. Sanavio, V. Peano, and A. Xuereb, Nonreciprocal topological phononics in optomechanical arrays, *Physical Review B* **101**, 085108 (2020).
- [26] H. Ren, T. Shah, H. Pfeifer, C. Brendel, V. Peano, F. Marquardt, and O. Painter, Topological phonon transport in an optomechanical system, *Nature Communications* **13**, 3476 (2022).
- [27] J. C. Budich and E. J. Bergholtz, Non-Hermitian Topological Sensors, *Phys. Rev. Lett.* **125**, 180403 (2020).

- [28] F. Koch and J. C. Budich, Quantum non-Hermitian topological sensors, *Phys. Rev. Res.* **4**, 013113 (2022).
- [29] J.-K. Wu, X.-W. Xu, H. Jing, L.-M. Kuang, F. Nori, and J.-Q. Liao, *Manipulating Topological Polaritons in Optomechanical Ladders* (2024), arXiv:2405.05753 [quant-ph].
- [30] E. J. Bergholtz, J. C. Budich, and F. K. Kunst, Exceptional topology of non-Hermitian systems, *Rev. Mod. Phys.* **93**, 015005 (2021).
- [31] K. Kawabata, K. Shiozaki, M. Ueda, and M. Sato, Symmetry and Topology in Non-Hermitian Physics, *Physical Review X* **9**, 041015 (2019).
- [32] T. A. Palomaki, J. D. Teufel, R. W. Simmonds, and K. W. Lehnert, Entangling mechanical motion with microwave fields., *Science* **342**, 710 (2013).
- [33] C. Genes, A. Mari, P. Tombesi, and D. Vitali, Robust entanglement of a micromechanical resonator with output optical fields, *Physical Review A* **78**, 032316 (2008).
- [34] G. A. Peterson, S. Kotler, F. Lecocq, K. Cicak, X. Y. Jin, R. W. Simmonds, J. Aumentado, and J. D. Teufel, Ultrastrong Parametric Coupling between a Superconducting Cavity and a Mechanical Resonator, *Physical Review Letters* **123**, 247701 (2019).
- [35] W. Brzezicki and T. Hyart, Hidden Chern number in one-dimensional non-Hermitian chiral-symmetric systems, *Physical Review B* **100**, 161105 (2019).
- [36] W. Brzezicki, M. Silveri, M. Płodzień, F. Massel, and T. Hyart, Non-Hermitian topological quantum states in a reservoir-engineered transmon chain, *Physical Review B* **107**, 115146 (2023).
- [37] M. Aspelmeyer, T. J. Kippenberg, and F. Marquardt, Cavity optomechanics, *Reviews of Modern Physics* **86**, 1391 (2014).
- [38] W. P. Bowen and G. J. Milburn, *Quantum Optomechanics*, CRC Press (CRC Press, 2015).
- [39] F. Marquardt, J. P. Chen, A. A. Clerk, and S. M. Girvin, Quantum theory of cavity-assisted sideband cooling of mechanical motion, *Physical Review Letters* **99**, 093902 (2007).
- [40] J. D. Teufel, T. Donner, D. Li, J. W. Harlow, M. S. Allman, K. Cicak, A. J. Sirois, J. D. Whittaker, K. W. Lehnert, and R. W. Simmonds, Sideband cooling of micromechanical motion to the quantum ground state, *Nature* **475**, 359 (2011).
- [41] M. Ludwig, B. Kubala, and F. Marquardt, The optomechanical instability in the quantum regime, *New Journal Of Physics* **10**, 095013 (2008).
- [42] F. Massel, T. T. Heikkilä, J. M. Pirkkalainen, S. U. Cho, H. Saloniemi, P. J. Hakonen, and M. A. Sillanpää, Microwave amplification with nanomechanical resonators, *Nature* **480**, 351 (2011).
- [43] A. H. Safavi-Naeini and O. Painter, Design of optomechanical cavities and waveguides on a simultaneous bandgap phononic-photon crystal slab, *Optics Express* **18**, 14926 (2010).
- [44] O. Painter, R. K. Lee, A. Scherer, A. Yariv, J. D. O'Brien, P. D. Dapkus, and I. Kim, Two-Dimensional Photonic Band-Gap Defect Mode Laser, *Science* **284**, 1819 (1999).
- [45] J. Vučković, M. Lončar, H. Mabuchi, and A. Scherer, Design of photonic crystal microcavities for cavity QED, *Physical Review E* **65**, 016608 (2002).
- [46] J. O. Vasseur, A.-C. Hladky-Hennion, B. Djafari-Rouhani, F. Duval, B. Dubus, Y. Pennec, and P. A. Deymier, Waveguiding in two-dimensional piezoelectric phononic crystal plates, *Journal of Applied Physics* **101**, 114904 (2007).
- [47] R. H. O. III and I. El-Kady, Microfabricated phononic crystal devices and applications, *Measurement Science and Technology* **20**, 012002 (2009).
- [48] Supplemental Material. Additional references appear in the supplemental material (Refs. [61–63]), (2024).
- [49] M. Eichenfield, J. Chan, R. M. Camacho, K. J. Vahala, and O. Painter, Optomechanical crystals, *Nature* **462**, 78 (2009).
- [50] M. Ludwig and F. Marquardt, Quantum Many-Body Dynamics in Optomechanical Arrays, *Physical Review Letters* **111**, 073603 (2013).
- [51] T. Prosen and T. H. Seligman, Quantization over boson operator spaces, *Journal of Physics A: Mathematical and Theoretical* **43**, 392004 (2010).
- [52] B. Bahari, A. Ndao, F. Vallini, A. E. Amili, Y. Fainman, and B. Kanté, Nonreciprocal lasing in topological cavities of arbitrary geometries, *Science* **358**, 636 (2017).
- [53] G. Harari, M. A. Bandres, Y. Lumer, M. C. Rechtsman, Y. D. Chong, M. Khajavikhan, D. N. Christodoulides, and M. Segev, Topological insulator laser: Theory, *Science* **359**, 10.1126/science.aar4003 (2018).
- [54] C. Metzger, M. Ludwig, C. Neuenhahn, A. Ortlieb, I. Favero, K. Karrai, and F. Marquardt, Self-Induced Oscillations in an Optomechanical System Driven by Bolometric Backaction, *Physical Review Letters* **101**, 133903 (2008).
- [55] F. Marquardt and S. Girvin, Optomechanics, *Physics* **2**, 40 (2009).
- [56] A. H. Safavi-Naeini, T. P. M. Alegre, J. Chan, M. Eichenfield, M. Winger, Q. Lin, J. T. Hill, D. E. Chang, and O. Painter, Electromagnetically induced transparency and slow light with optomechanics, *Nature* **472**, 69 (2011).
- [57] G. Adesso and F. Illuminati, Entanglement in continuous-variable systems: recent advances and current perspectives, *Journal of Physics A: Mathematical and Theoretical* **40**, 7821 (2007).
- [58] M. Abdi, S. Barzanjeh, P. Tombesi, and D. Vitali, Effect of phase noise on the generation of stationary entanglement in cavity optomechanics, *Physical Review A* **84**, 032325 (2011).
- [59] S. G. Hofer, W. Wieczorek, M. Aspelmeyer, and K. Hammerer, Quantum entanglement and teleportation in pulsed cavity optomechanics, *Physical Review A* **84**, 052327 (2011).
- [60] D. Vitali, S. Gigan, A. Ferreira, H. R. Böhm, P. Tombesi, A. Guerreiro, V. Vedral, A. Zeilinger, and M. Aspelmeyer, Optomechanical Entanglement between a Movable Mirror and a Cavity Field, *Physical Review Letters* **98**, 030405 (2007).
- [61] C. W. Gardiner and P. Zoller, *Quantum noise*, Springer (Springer, 2004).
- [62] C. W. Gardiner, *Handbook of Stochastic Methods for Physics, Chemistry and the Natural Sciences*, Springer Series in Synergetics (Springer series in synergetics, 2004).
- [63] D. F. Walls and G. J. Milburn, *Quantum Optics*, Quantum Optics (Springer Berlin Heidelberg, 2008).

Non-hermitian topology in optomechanics – Supplemental material

Wojciech Brzezicki,^{1,2} Timo Hyart,^{3,4} and Francesco Massel⁵

¹*Institute of Theoretical Physics, Jagiellonian University,
ulica S. Łojasiewicza 11, PL-30348 Kraków, Poland*

²*International Research Centre MagTop, Institute of Physics,
Polish Academy of Sciences, Aleja Lotników 32/46, PL-02668 Warsaw, Poland*

³*Computational Physics Laboratory, Physics Unit,
Faculty of Engineering and Natural Sciences, Tampere University, FI-33014 Tampere, Finland*

⁴*Department of Applied Physics, Aalto University, 00076 Aalto, Espoo, Finland*

⁵*Department of Science and Industry Systems, University of South-Eastern Norway, PO Box 235, Kongsberg, Norway*

CONTENTS

I. Linearized optomechanical Hamiltonian: derivation	1
II. Dynamical system equations	3
III. Stability, covariance matrix, entanglement	3
IV. PBC and OBC spectra	5
V. Non-Hermitian topology	7
VI. Two-site model	8
VII. Topological protection	9
A. Hopping disorder	9
B. On-site frequency disorder	11
C. End-sites mechanical dissipation renormalization	13
VIII. Third quantization approach	13
A. Hamiltonian	13
B. Liouvillian	14
C. Time-evolution	15
D. Solution of the Lyapunov equation	16
E. Correlation functions	16
F. Non-zero temperature	17
G. Stationary correlation matrix	17
H. Entanglement in the presence of unstable end modes	18
IX. Entanglement measurement	19
References	21

I. LINEARIZED OPTOMECHANICAL HAMILTONIAN: DERIVATION

We consider here a 1D lattice of optomechanical systems whose phononic degrees of freedom are coupled through a hopping Hamiltonian. Namely

$$H_{\text{opt}} = \sum_{i=0}^N H_i + H_J \quad (1)$$

with

$$\begin{aligned}
H_i &= \omega_{c,i} a_i^\dagger a_i + \omega_{m,i} b_i^\dagger b_i + g_i a_i^\dagger (b_i^\dagger + b_i) \\
H_J &= -J \sum_{i=0}^N (b_i^\dagger b_{i+1} + \text{h.c.})
\end{aligned} \tag{2}$$

where, for each site i a_i , b_i are the photonic and mechanical degrees of freedom, with resonant frequencies given by $\omega_{c,i}$ and $\omega_{m,i}$, respectively, and J the hopping energy. This setup could be realized, for instance, in an optomechanical crystal. The experimental realization of optomechanical crystals was first discussed in Ref. [1], building upon previous work in the context of photonic [2, 3] and phononic [4, 5] crystals. While the concomitant presence of hopping both for optical and mechanical degrees of freedom can be included in our analysis, analogously to what was discussed in Ref. [6], we focus here on the case of purely mechanical hopping.

In our analysis, we assume that all sites are identical ($\omega_{c,i} = \omega_c$, $\omega_{m,i} = \omega_m$, $g_i = g$). Along the lines of [7], where the coupling to the environment of a 1D transmon chain was modified to obtain a periodic modulation of the dissipation properties, we consider here a spatial-dependent drive of the optomechanical chain in a BRRB pattern. Each site of the chain is either driven on the blue (“B”) or the red (“R”) sideband [8].

The linearization of the equations of motion (EOMs) generated by $H_i + H_J$, in the presence of an external drive modeled by $H_d = \alpha_d e^{-i\omega_d t}$ can be performed with the same strategy used to linearize the Hamiltonian of a single optomechanical system. Focusing on site i the EOMs for a_i and b_i can be written as

$$\dot{a}_i = -i\omega_c a_i - ig_0 a_i (b_i^\dagger - \frac{\kappa}{2} a_i - \alpha_d e^{-i\omega_d t} + b_i) + \sqrt{\kappa} a_{\text{in},i} \tag{3a}$$

$$\dot{b}_i = -i\omega_m b_i - ig_0 a_i^\dagger a_i + iJ(b_{i+1} + b_{i-1}) - \frac{\gamma}{2} b_i + \sqrt{\gamma} b_{\text{in},i} \tag{3b}$$

Writing the optical and mechanical operators as a combination of a strong classical tone imposed by the drive α_d and of a quantum fluctuation. Namely,

$$a_i \rightarrow \alpha_i + a_i, \quad b_i \rightarrow \beta_i + b_i.$$

We can solve Eqs. (25,26) order-by-order. The zeroth order is given by

$$\dot{\alpha}_i = i\Delta \alpha_i - \frac{\kappa}{2} \alpha_i - \alpha_d - ig_0 \alpha_d (\beta_i^* + \beta_i) \tag{4a}$$

$$\dot{\beta}_i = -i\omega_m \beta_i - \frac{\kappa}{2} \beta_i - ig_0 |\alpha_d|^2 + iJ (\beta_{i+1} + \beta_{i-1}), \tag{4b}$$

where we have moved to a frame rotating at the external drive frequency ω_d and $\Delta = \Omega_d - \Omega_c$. Since the drive imposes a constant displacement to the cavity and the mechanical field (in the frame rotating at ω_d), we have $\dot{\alpha}_i = 0$ and $\dot{\beta}_i = 0$, allowing us to solve Eqs. (4a,4b) as a set of coupled algebraic equations. We note here that, if g_0 (and the mechanical displacement) are sufficiently small, namely $g_0 (\beta_i^* + \beta_i) \ll \Delta$, the equations for the cavity field can be solved independently from the mechanical degrees of freedom.

The first-order equations can be written as

$$\dot{a}_i = -\frac{\kappa}{2} a_i - ig_0 \alpha_i e^{-i\Delta t} (e^{i\omega_m t} b_i^\dagger + e^{-i\omega_m t} b_i) + \sqrt{\kappa} a_{\text{in},i} \tag{5a}$$

$$\dot{b}_i = -\frac{\gamma}{2} b_i - ig_0 e^{i\omega_m t} (\alpha_i e^{-i\Delta t} a_i^\dagger + \alpha_i^* e^{i\Delta t} a_i) + iJ (b_{i+1} + b_{i-1}) + \sqrt{\gamma} b_{\text{in},i} \tag{5b}$$

where we have now moved to a frame rotating at the cavity frequency ω_c and at the mechanical frequency ω_m for a_i and b_i , respectively. We now consider two specific values for the driving frequency ω_d . The first one is such as to fulfill the condition $\bar{\Delta} = -\omega_m$ (red-detuned drive). Invoking the rotating wave approximation, we are allowed to neglect in Eqs. (5a,5b) fast oscillating terms that oscillate at $\bar{\Delta} - \omega_m \simeq 2\omega_m$. With this approximation, Eqs. (5a,5b) become

$$\dot{a}_i = -\frac{\kappa}{2} a_i - iG_- b_i + \sqrt{\kappa} a_{\text{in},i} \tag{6a}$$

$$\dot{b}_i = -\frac{\gamma}{2} b_i - iG_- a_i + iJ (b_{i+1} + b_{i-1}) + \sqrt{\gamma} b_{\text{in},i} \tag{6b}$$

where and we have used the fact that $\bar{\Delta} + \omega_m = 0$ and assumed, without loss of generality that $G_- = g_0 \alpha_i$. Conversely, choosing ω_d , in such a way that $\bar{\Delta} = \omega_m$ (blue-detuned drive), leads to the following EOMs

$$\dot{a}_i = -\frac{\kappa}{2} a_i - iG_+ b_i^\dagger + \sqrt{\kappa} a_{\text{in},i} \tag{7a}$$

$$\dot{b}_i = -\frac{\gamma}{2} b_i - iG_+ a_i^\dagger + iJ (b_{i+1} + b_{i-1}) + \sqrt{\gamma} b_{\text{in},i}. \tag{7b}$$

The EOMs given in Eqs. (6a-7b) can be thought of as originating from the following bilinear Hamiltonians (in the laboratory frame)

$$\begin{aligned} H_{i,R} &= \omega_c a_i^\dagger a_i + \omega_m b_i^\dagger b_i + G_- a_i^\dagger b_i + J(b_i^\dagger b_{i+1} + b_i^\dagger b_{i-1}) \text{ h.c.} \\ H_{i,B} &= \omega_c a_i^\dagger a_i + \omega_m b_i^\dagger b_i + G_+ a_i^\dagger b_i^\dagger + J(b_i^\dagger b_{i+1} + b_i^\dagger b_{i-1}) + \text{ h.c.} \end{aligned} \quad (8)$$

depending on whether site i is driven on the red or the blue sideband, respectively. These two Hamiltonians are the building blocks for the Hamiltonian given in Eq.(1) of the main text.

II. DYNAMICAL SYSTEM EQUATIONS

We consider here the dynamics induced by the Hamiltonian (26) in the presence of a coupling to thermal reservoirs both for the mechanical and the optical degrees of freedom, introducing dissipation rates γ and κ and noise operators $b_{\text{in},i}$ and $a_{\text{in},i}$ for the mechanical and optical degrees of freedom, respectively. The operators $b_{\text{in},i}$ fulfill the following relations

$$\langle b_{\text{in},i}(t) b_{\text{in},i}^\dagger(t') \rangle = (n_m + 1) \delta(t - t') \quad (9a)$$

$$\langle b_{\text{in},i}^\dagger(t) b_{\text{in},i}(t') \rangle = n_m \delta(t - t') \quad (9b)$$

and analogous relations hold for $a_{\text{in},i}$

$$\langle a_{\text{in},i}(t) a_{\text{in},i}^\dagger(t') \rangle = (n_c + 1) \delta(t - t') \quad (10a)$$

$$\langle a_{\text{in},i}^\dagger(t) a_{\text{in},i}(t') \rangle = n_c \delta(t - t'). \quad (10b)$$

The Hamiltonian given Eq. (1) of the main text generates the following dynamics, described by the quantum Langevin equations (QLEs) [9], for the optical and mechanical degrees of freedom

$$\dot{a}_i = -i [a_i, \hat{H}] - \frac{\kappa}{2} a_i + \sqrt{\kappa} a_{i,\text{in}} \quad (11a)$$

$$\dot{b}_i = -i [b_i, \hat{H}] - \frac{\gamma}{2} b_i + \sqrt{\gamma} b_{i,\text{in}}. \quad (11b)$$

Eqs.(11a,11b) can be written more compactly in terms of a operators vector $\mathbf{a} = [a_1, b_1, \dots, a_{4N}, b_{4N}; a_1^\dagger, b_1^\dagger, \dots, a_{4N}^\dagger, b_{4N}^\dagger]^T$

and an input-operators vector $\mathbf{a}_{\text{in}} = [a_{\text{in}1}, b_{\text{in}1}, \dots, a_{\text{in}4N}, b_{\text{in}4N}; a_{\text{in}1}^\dagger, b_{\text{in}1}^\dagger, \dots, a_{\text{in}4N}^\dagger, b_{\text{in}4N}^\dagger]^T$

$$\dot{\mathbf{a}} = -i \mathcal{H}_{\text{NH}} \mathbf{a} + \sqrt{\bar{\eta}} \mathbf{a}_{\text{in}} \quad (12)$$

with $\bar{\eta} = \text{diag}(\kappa, \gamma, \dots; \kappa, \gamma, \dots, \kappa, \gamma)$, and

$$\mathcal{H}_{\text{NH}} = \bar{\sigma}_z \mathcal{H} - \frac{i\bar{\eta}}{2} \quad (13)$$

where $\bar{\sigma}_z = \text{diag}(1, \dots, 1; -1, \dots, -1)$. The solution of Eq. (12) can be written as

$$\mathbf{a} = \exp[-i \mathcal{H}_{\text{NH}} t] \mathbf{a}_0 + \int_0^t \exp[-i \mathcal{H}_{\text{NH}}(t - \tau)] \sqrt{\bar{\eta}} \mathbf{a}_{\text{in}} d\tau, \quad (14)$$

which corresponds to Eq. (2) of the main text.

III. STABILITY, COVARIANCE MATRIX, ENTANGLEMENT

The first aspect in the study of the (quantum) dynamical system described by Eq. (12), whose solution is given by Eq. (14) (Eq. (2) of the main text) is its stability. Eq. (12) can be construed as a quantum stochastic differential equation [9] (quantum version of a Ornstein-Uhlenbeck process [10]), which can be written, in general, as

$$\dot{\hat{a}} = A \bar{a} + \bar{\xi}_{\text{in}}. \quad (15)$$

Its stability is guaranteed by the condition $\text{Re } \lambda_i < 0$ where λ_i are the eigenvalues of the matrix associated with the dynamical system, in our case $A = -i\mathcal{H}_{\text{NH}}$. This condition corresponds to the $\text{Im } E < 0$ condition on the eigenenergies of the non-Hermitian Hamiltonian \mathcal{H}_{NH} .

From Eq. (15), it is possible to write the Lyapunov equation for the time evolution of the covariance matrix V for the operators $[a_1, b_1, a_1^\dagger, b_1^\dagger, \dots]$, namely

$$\frac{dV_{\bar{a},\bar{a}^\dagger}}{dt} = AV_{\bar{a},\bar{a}^\dagger} + V_{\bar{a},\bar{a}^\dagger}A^\dagger + D \quad (16)$$

where

$$V_{\bar{a},\bar{a}^\dagger} = \begin{bmatrix} \langle a_1 a_1^\dagger \rangle & \langle a_1 b_1^\dagger \rangle & \langle a_1 a_1 \rangle & \langle a_1 b_1 \rangle & \dots \\ \langle b_1 a_1^\dagger \rangle & \dots & & & \\ \vdots & & & & \end{bmatrix}$$

and $D = \text{diag}[\kappa(n_a + 1), \gamma(n_b + 1), \kappa n_a, \gamma n_b, \dots]$. In our analysis, we are interested in the stationary value of the covariance matrix. We therefore seek a numerical solution to the equation

$$AV_{\bar{a},\bar{a}^\dagger} + V_{\bar{a},\bar{a}^\dagger}A^\dagger + D = 0. \quad (17)$$

From $V_{\bar{a},\bar{a}^\dagger}$ it is possible to obtain the covariance matrix between the quadratures –either mechanical

$$\begin{aligned} X_{\text{m},i} &= 1/\sqrt{2} (b_i^\dagger + b_i), \\ P_{\text{m},i} &= i/\sqrt{2} (b_i^\dagger - b_i) \end{aligned}$$

or optical

$$\begin{aligned} X_{\text{o},i} &= 1/\sqrt{2} (a_i^\dagger + a_i), \\ P_{\text{o},i} &= i/\sqrt{2} (a_i^\dagger - a_i). \end{aligned}$$

We evaluate the entanglement properties between the quadratures $\xi, \eta = \text{m, c}$ on sites i, j , considering the two mode covariance matrix

$$V_{\xi,i,\eta,j} = \begin{bmatrix} \langle X_{\xi,i} X_{\xi,i} \rangle & \langle X_{\xi,i} P_{\xi,i} \rangle & \langle X_{\xi,i} X_{\eta,j} \rangle & \langle X_{\xi,i} P_{\eta,j} \rangle \\ \langle P_{\xi,i} X_{\xi,i} \rangle & \langle P_{\xi,i} P_{\xi,i} \rangle & \langle P_{\xi,i} X_{\eta,j} \rangle & \langle P_{\xi,i} P_{\eta,j} \rangle \\ \langle X_{\eta,i} X_{\xi,i} \rangle & \langle X_{\eta,i} P_{\xi,i} \rangle & \langle X_{\eta,i} X_{\eta,j} \rangle & \langle X_{\eta,i} P_{\eta,j} \rangle \\ \langle P_{\eta,i} X_{\xi,i} \rangle & \langle P_{\eta,i} P_{\xi,i} \rangle & \langle P_{\eta,i} X_{\eta,j} \rangle & \langle P_{\eta,i} P_{\eta,j} \rangle \end{bmatrix}. \quad (18)$$

Eq. (18) can be written in terms of three 2×2 matrices α, β, γ as

$$V_{i,j} = \begin{bmatrix} \alpha_{i,j} & \gamma_{i,j} \\ \gamma_{i,j}^T & \beta_{i,j} \end{bmatrix} \quad (19)$$

Following [11], we can determine the negativity associated with the entanglement (or lack thereof).

The positivity of the partial transposed state (PPT criterion) can be recast as the condition $\tilde{\nu}_- \geq 1$ on the smallest symplectic eigenvalue of the covariance matrix evaluated on the partially transposed state. These can be expressed in terms of Eq. (19) as

$$\tilde{\nu}_\pm = \sqrt{\frac{\tilde{\Delta}_{i,j} \pm \sqrt{\tilde{\Delta}_{i,j}^2 - 4 \text{Det } V_{i,j}}}{2}} \quad (20)$$

where $\tilde{\Delta}_{i,j} = \text{Det } \alpha_{i,j} + \text{Det } \beta_{i,j} - 2 \text{Det } \gamma_{i,j}$.

The (logarithmic) negativity

$$E_{\mathcal{N}} = \max[0, -\log_2 \tilde{\nu}_-] \quad (21)$$

gives a measure of the violation of the condition $\tilde{\nu}_- \geq 1$, and thus quantifies the entanglement between the modes localized on sites i and j . Furthermore, the diagonal elements of $V_{\xi,i,\eta,j}$ allow us to infer the number of mechanical excitations on sites i and j .

IV. PBC AND OBC SPECTRA

We depict here the spectra for periodic and open boundary conditions for different values of G_+ . In Fig. 1, we consider the case where both end states are stable. Panel 1(a) illustrates the case for which $\text{Im}E_e$ is within the $\text{Im}E_b$ band ($G_+ = 0.2$), whereas panel 1(b) refers to the case $G_+ = 0.446$, for which a gap develops between $\text{Im}E_e \rightarrow 0^-$ and $\text{Im}E_b < 0$ states.

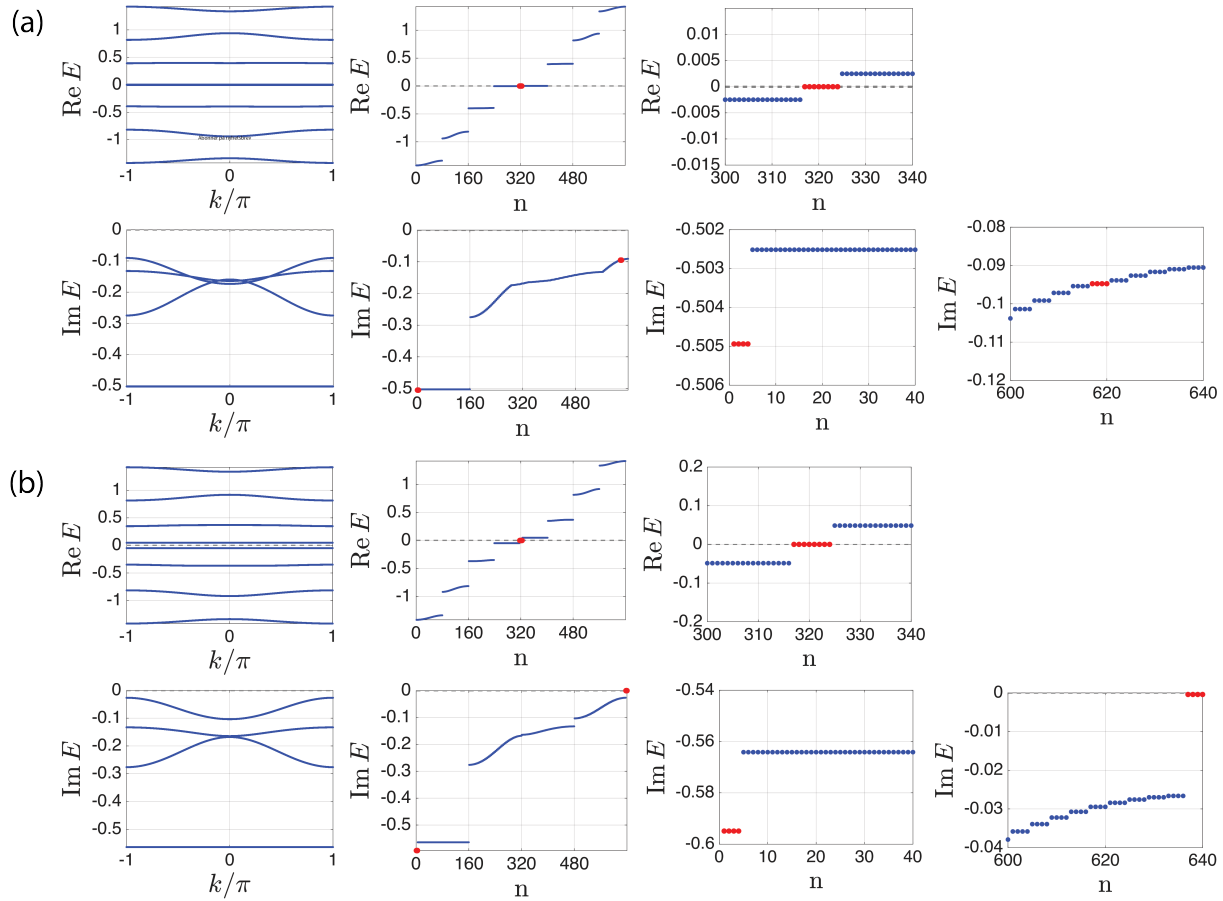


Figure 1. Real and imaginary spectra for periodic (first column) and open (second column) boundary conditions (columns three and four represent a zoom-in of column two). Red dots correspond to $\text{Im}E_e < 0$, i.e. (stable) end states, blue dots to $\text{Im}E_b$, i.e. bulk states. (a) $G_+ = 0.2$, (b) $G_+ = 0.446$. $G_- = 1$, $J = 0.5$, $\gamma = 10^{-4}$ (all energies expressed in units of κ). For $G_+ = 0.446$, $\text{Im}E_e \simeq 4 \cdot 10^{-4}$.

In Fig. 2, we further increase G_+ . At first ($G_+ = 0.26$, panel 2(a)) end states become unstable, while bulk states are still stable. Further increasing G_+ ($G_+ = 0.35, G_+ = 1$) leads the instability of the bulk states as well. The case $G_+ = 0.35$ (panel 2(b)) corresponds to the case for which both the PBC and the OBC spectra are gapless at $\text{Im}E = 0$, while a gap develops for $G_+ = 1$ (anel 2(c))

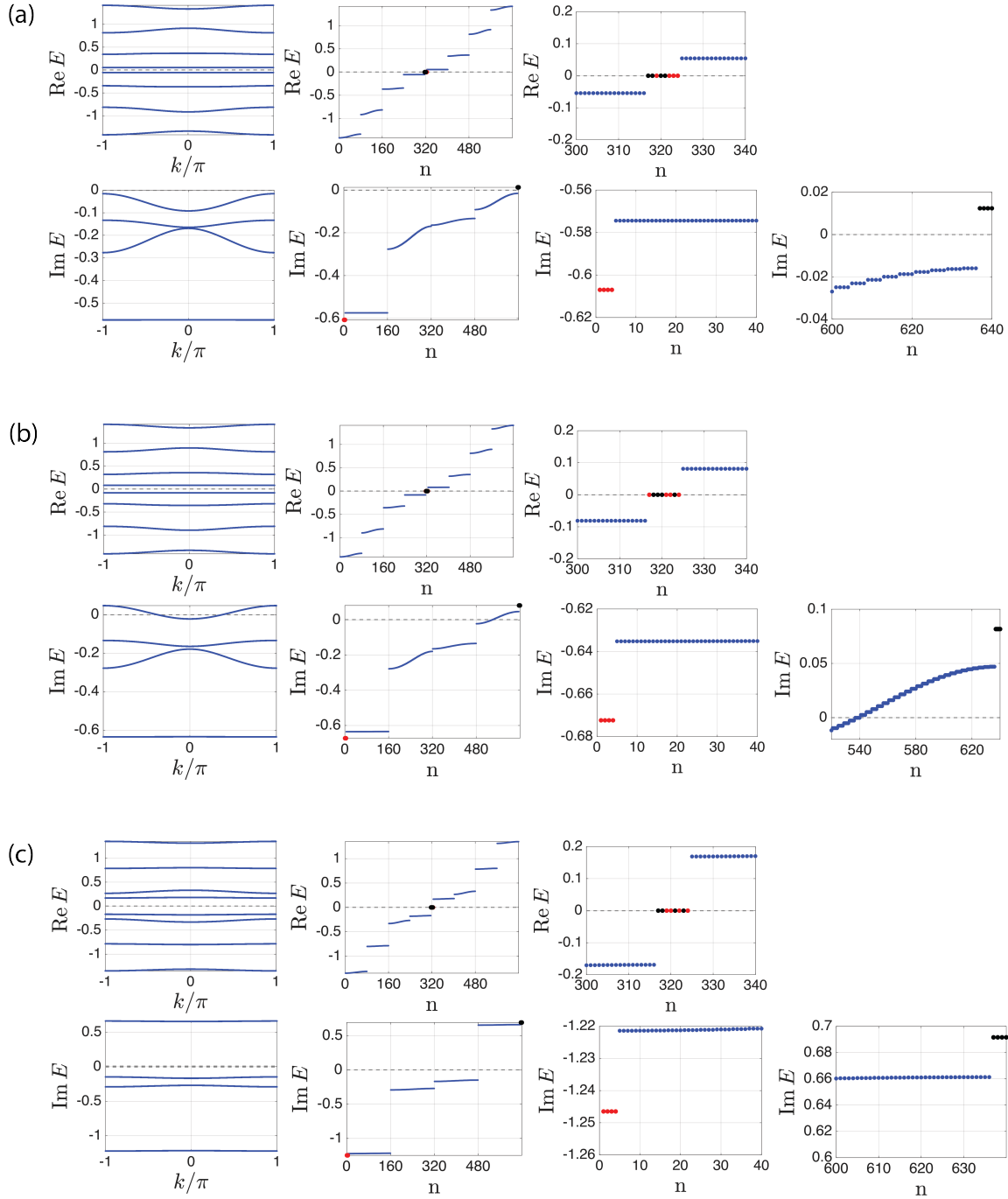


Figure 2. Real and imaginary spectra for periodic (first column) and open (second column) boundary conditions (columns three and four represent a zoom-in of column two). Red dots correspond to $\text{Im}E_e < 0$, i.e. stable end states, black dots correspond to $\text{Im}E_e > 0$, i.e. unstable end states, blue dots to $\text{Im}E_b$, i.e. bulk states. (a) $G_+ = 0.35$, (b) $G_+ = 1$. $G_- = 1, J = 0.5, \gamma = 10^{-4}$ (all energies expressed in units of κ).

V. NON-HERMITIAN TOPOLOGY

In order to establish the topological character of the (complex) spectrum of the chain, we rely on the analysis performed in Ref. [12], where, as outlined in the main text, the authors establish an exact mapping between the complex spectrum at $\text{Re } E = 0$ of a non-hermitian Hamiltonian—in our case \mathcal{H}_{NH} —and an effective hermitian Hamiltonian given by

$$\mathcal{H}_{\text{eff}}(\eta, k) = \eta S - iS\mathcal{H}_{\text{NH}}(k).$$

The definition of S originates from the symmetry properties of \mathcal{H}_{NH} : it is possible to show that \mathcal{H}_{NH} obeys a non-hermitian chiral symmetry

$$S\mathcal{H}_{\text{NH}}S^{-1} = -\mathcal{H}_{\text{NH}}^\dagger \quad (22)$$

where $S = \Pi\Sigma$,

$$\Sigma = \begin{pmatrix} \sigma & 0 & 0 & 0 \\ 0 & \sigma & 0 & 0 \\ 0 & 0 & \sigma & 0 \\ 0 & 0 & 0 & \sigma \end{pmatrix}, \quad \Pi = \begin{pmatrix} \sigma & 0 & 0 & 0 \\ 0 & \tau & 0 & 0 \\ 0 & 0 & -\tau & 0 \\ 0 & 0 & 0 & -\sigma \end{pmatrix},$$

$\sigma = \sigma_z \otimes \mathbb{I}_2$, $\tau = \mathbb{I}_2 \otimes \sigma_z$, and σ_z is the 2x2 Pauli matrix.

We focus on the eigenstates ψ of \mathcal{H}_{NH} with $\text{Re} = 0$ (for open boundary conditions). The states ψ must therefore satisfy the following relation

$$\mathcal{H}_{\text{NH}}\psi = i\eta\psi. \quad (23)$$

From the symmetry properties expressed in Eq. (22), it is possible to show that Eq. (23) can be recast as a zero-energy eigenproblem for the *hermitian* Hamiltonian \mathcal{H}_{eff} . Namely

$$\mathcal{H}_{\text{eff}}(\psi, k)\psi \doteq S(\eta - i\mathcal{H}_{\text{NH}})\psi = 0. \quad (24)$$

The potentially nontrivial topological properties of $\mathcal{H}_{\text{eff}}(k, \eta)$ are reflected into the topological protection of the $\text{Re} = 0$ (end) modes of \mathcal{H}_{NH} . To ascertain the topological protection of the end modes, following [7], we can evaluate the Berry curvature and the Chern number associated with \mathcal{H}_{eff} as

$$\Omega_{k,\eta} = \sum_{\substack{n \leq s \\ m > s}} \text{Im} \frac{2 \left[\psi_{k,\eta}^{n*} (\partial_k \mathcal{H}_{\text{eff}}) \psi_{k,\eta}^m \right] \left[\psi_{k,\eta}^{m*} (\partial_\eta \mathcal{H}_{\text{eff}}) \psi_{k,\eta}^n \right]}{\left(E_{k,\eta}^{(n)} - E_{k,\eta}^{(m)} \right)^2} \quad (25)$$

and

$$C = \frac{1}{2\pi} \int_{-\infty}^{+\infty} d\eta \int_0^{2\pi} dk \Omega_{k,\eta}, \quad (26)$$

where the eigenstates are sorted in ascending order of the eigenenergy. In order to guarantee the quantization of the Chern number for $\mathcal{H}_{\text{eff}}(k, \eta)$, one has to require its periodicity in k and η . While the periodicity of the former is guaranteed by the periodicity of $\mathcal{H}_{\text{NH}}(k)$, $\mathcal{H}_{\text{eff}}(k, \eta)$ is not periodic in η . This issue can be solved by defining a compactified version of $\mathcal{H}_{\text{eff}}(k, \eta)$, sharing with it the same spectrum, through the relation

$$\mathcal{H}_{\text{eff}}^{\text{cmp}}(k, \eta) = \mathcal{R}_\eta \mathcal{H}_{\text{eff}}(k, \eta) \mathcal{R}_\eta^\dagger \quad (27)$$

with

$$\mathcal{R}_\eta = \exp \left[i \frac{\pi}{4} (1 + \tanh \eta) \mathcal{G} \right], \quad \mathcal{G} = \begin{pmatrix} & & & \mathbb{I}_4 \\ & & & \\ & & \mathbb{I}_4 & \\ & & & \\ \mathbb{I}_4 & & & \end{pmatrix} \quad (28)$$

VI. TWO-SITE MODEL

The stability and dissipation properties of the end states can be approximated terms of dynamics of a two-site system, with one site driven on the blue sideband (G_+) and the other on the red (G_-). Intuitively, this setup corresponds to G_- -driven site acting as an effective bath for the G_+ driven one, stabilizing its dynamics. In Fourier space, the dynamics of the two-site system can be written as

$$\mathbf{a} = A \xi_{\text{in}} \quad (29)$$

where $\mathbf{a} = [a_1, b_1^\dagger, a_2, b_2]$, $\xi_{\text{in}} = [\sqrt{\kappa} a_{\text{in},1}, \sqrt{\gamma} b_{\text{in},1}^\dagger, \sqrt{\kappa} a_{\text{in},2}, \sqrt{\gamma} b_{\text{in},2}]$ and

$$A^{-1} = \begin{pmatrix} \chi_c^{-1} & iG_+ & 0 & 0 \\ -iG_+ & \chi_m^{-1} & 0 & -iJ \\ 0 & 0 & \chi_c^{-1} & -iG_- \\ 0 & -iJ & -iG_- & \chi_m^{-1} \end{pmatrix} \quad (30)$$

with $\chi_m = (\gamma/2 - i\omega)^{-1}$ and $\chi_c = (\kappa/2 - i\omega)^{-1}$. With an analysis similar to the one carried out in Sec. II, it is possible to show that the poles of the matrix A correspond to the (complex) excitation energies for the two-site system, and, in particular, their imaginary part characterizes its stability properties. In Fig. 3 we compare the complex eigenenergies of the two-site system, with the spectrum of the chain, and we see that the overall behavior of the end state (in red) is well captured by the two-site description. While an analytical solution to the two-site problem is possible the expressions for $\text{Im}E_{2\text{-site}}$ are not particularly informative. We provide here the expression for $\text{Im}E_{2\text{-site}}$ corresponding to the largest imaginary part of the two-site eigenenergies in the limit $G_+ \rightarrow 0$ and $G_+ \rightarrow \infty$. For $G_+ \rightarrow 0$ we have

$$\text{Im} E_{2\text{-site}} \simeq -\frac{\Delta^{1/3} + \kappa + 2\gamma}{6} + \frac{12(G_-^2 + J^2) - (\kappa - \gamma)^2}{6\Delta^{1/3}} \quad (31)$$

with

$$\Delta = \kappa (\kappa^2 - 18G_-^2 + 36J^2) + \sqrt{\kappa^2 (\kappa^2 - 18G_-^2 + 36J^2)^2 - (\kappa^2 - 12G_-^2 - 12J^2)^3} - 3(\kappa^2 - 6G_-^2 + 12J^2)\gamma + O(\gamma^2)$$

which, expanding in powers of J/G_- , can be written as

$$\text{Im} E_{2\text{-site}} \simeq -\frac{\gamma}{2} - (\kappa - \gamma) \frac{J^2}{G_-^2} \left(1 - \frac{J^2}{G_-^2}\right) + O\left[\left(\frac{J}{G_-}\right)^5\right] \quad (32)$$

Conversely, for $G_+ \rightarrow \infty$ we get

$$\text{Im} E_{2\text{-site}} \simeq -\frac{\kappa + \gamma}{2} + \sqrt{\frac{(\kappa - \gamma)^2}{4} + 4G_+^2}. \quad (33)$$

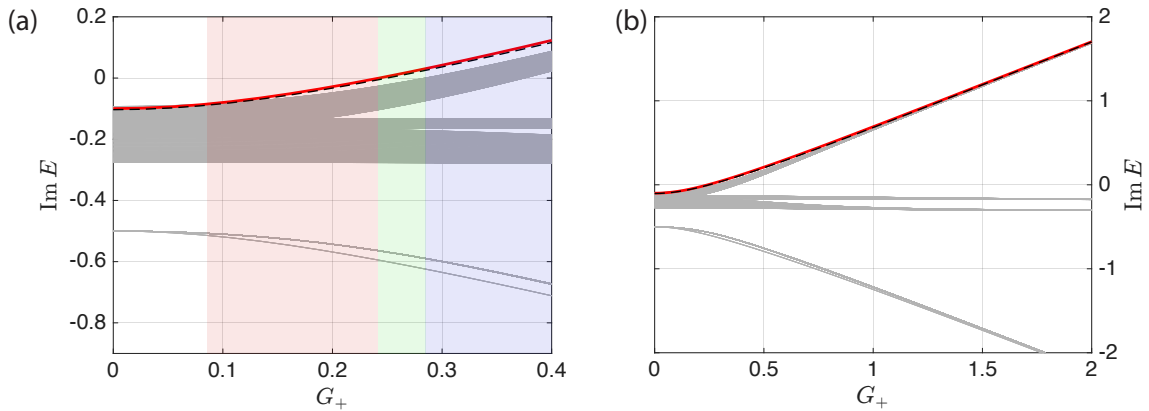


Figure 3. Imaginary part of the OBC spectrum $\text{Im}E$ as a function of G_+ . Red line: $\text{Im} E_e$; dashed line: approximate result given by the solution of the two-site problem. (a) $G_+ \in [0, 0.4]$ corresponding to Fig. 3 of the main text. (b) $G_+ \in [0, 2]$. $G_-, J = 0.5$, $\gamma \leq 10^{-4}$ (all energies expressed in units of κ).

VII. TOPOLOGICAL PROTECTION

A. Hopping disorder

We plot here the spectra (for periodic- and open-boundary conditions) in the presence of disorder for the hopping parameter J (δJ uniformly distributed in $[-0.1J, 0.1J]$), for different values of G_+ . For all values of G_+ it is possible to see that the $\text{Re } E = 0$ end states survive in the presence of disorder. The degeneracy of $\text{Im } E$, however, is partially lifted: the imaginary part of the spectrum shows the appearance of pairs of states instead of the quadruplet associated with the corresponding spectrum in the absence of disorder.

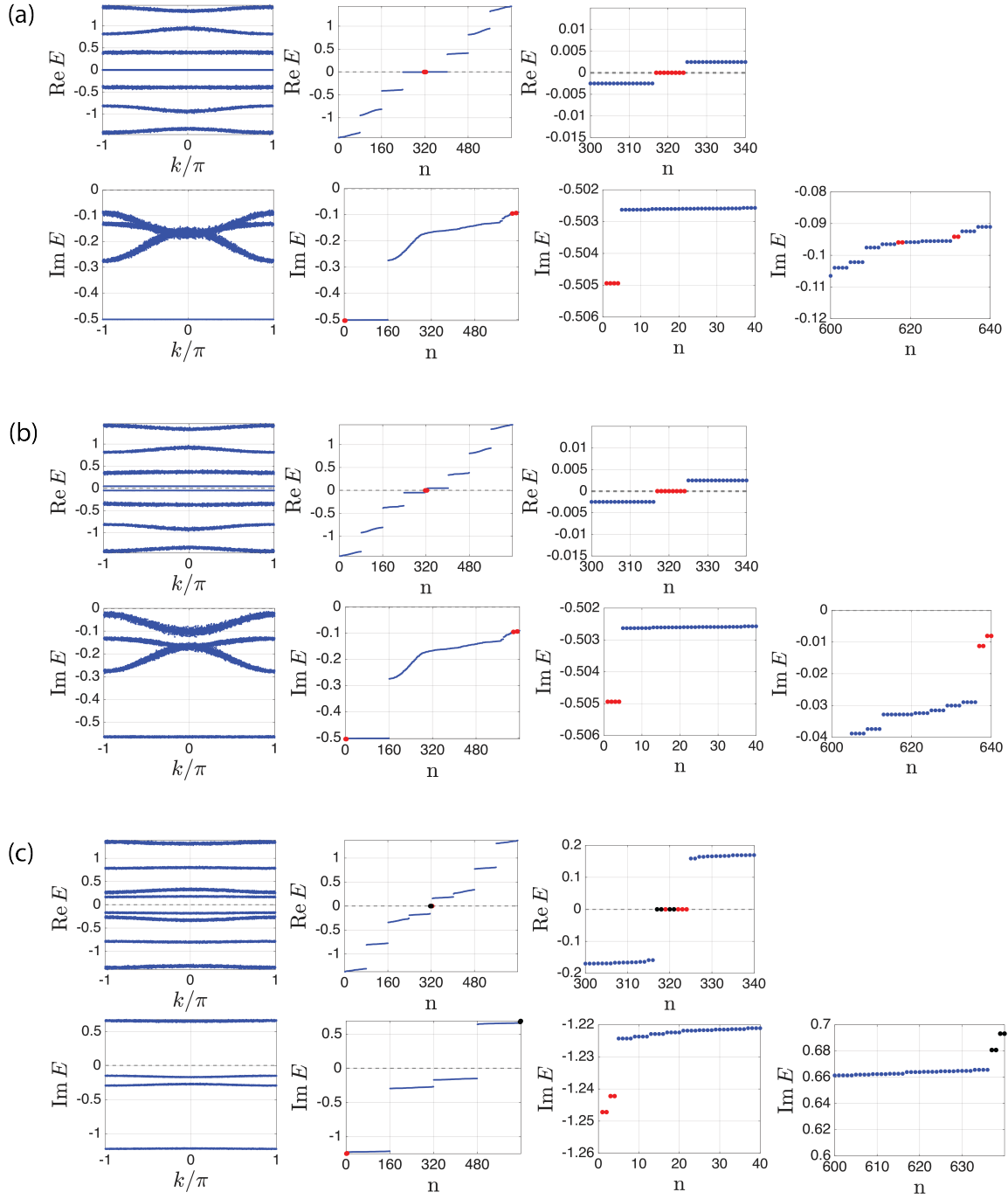


Figure 4. Real and imaginary spectra for periodic (first column) and open (second column) boundary conditions (columns three and four represent a zoom-in of column two). Red dots correspond to $\text{Im } E_e < 0$, i.e. stable end states, black dots correspond to $\text{Im } E_e > 0$, i.e. unstable end states, blue dots to $\text{Im } E_b$, i.e. bulk states. (a) $G_+ = 0.05$, (b) $G_+ = 0.242$, (c) $G_+ = 1$. $G_- = 1$, $J = 0.5$, $\gamma = 10^{-4}$, $\delta J/J = 0.1$ (all energies expressed in units of κ).

B. On-site frequency disorder

We take here into account the potential difference of on-site frequencies for either the mechanics or the cavity. Following the derivation in section I it is easy to show that a site dependence of ω_c can be absorbed into the choice of the driving frequency ω_d . Conversely, a potential site dependence of the mechanical frequency has to be explicitly taken into account. In Fig. 5, we have plotted the spectra for ω_m uniformly distributed (in the rotating frame) in $[-0.01\omega_m, 0.01\omega_m]$. The disorder amplitude is compatible with the current experimental capabilities discussed in [13].

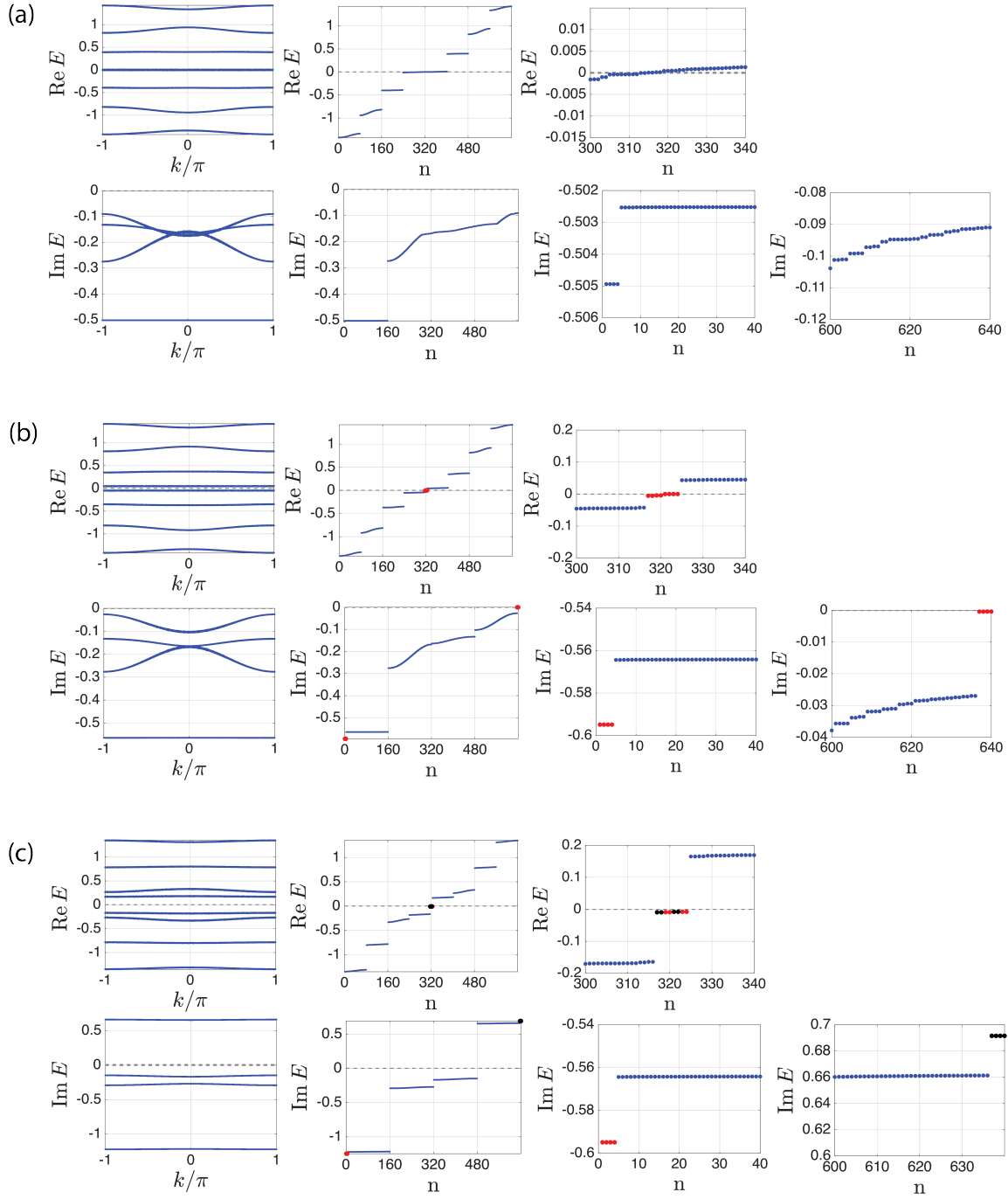


Figure 5. Real and imaginary spectra for periodic (first column) and open (second column) boundary conditions (columns three and four represent a zoom-in of column two). Red dots correspond to $\text{Im}E_e < 0$, i.e. stable end states, black dots correspond to $\text{Im}E_e > 0$, i.e. unstable end states, blue dots to $\text{Im}E_b$, i.e. bulk states. (a) $G_+ = 0.05$, (b) $G_+ = 0.242$, (c) $G_+ = 1$. $G_- = 1$, $J = 0.5$, $\gamma = 10^{-4}$, $\delta\omega_m/\omega_m = 0.01$ (all energies expressed in units of κ).

As expected from the breaking of the chiral symmetry, Fig 5 displays a deviation from the $\text{Re} E = 0$ condition for the end states. For the parameters considered here, however, the real part of the spectrum still exhibits a significant gap for the $\text{Re} E \neq 0$ states.

C. End-sites mechanical dissipation renormalization

We depict here the OBC spectra in the presence of measurement-induced renormalization of the end-states mechanical dissipation. As expected, in these figures it is possible to see that even for $\gamma_{\text{end}} = 100\gamma$, the spectrum is essentially unchanged, as expected from a topological protection argument.

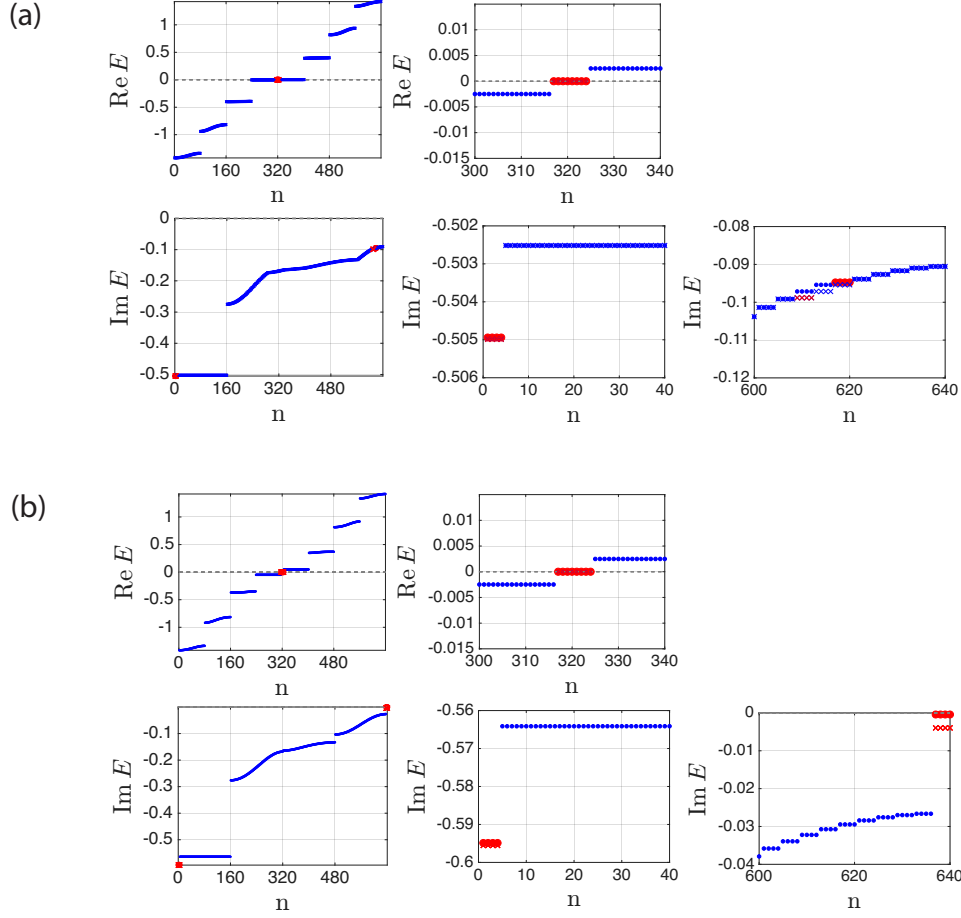


Figure 6. Real and imaginary spectra for periodic (first column) and open (second column) boundary conditions (columns three and four represent a zoom-in of column two). Red dots correspond to $\text{Im}E_e < 0$, i.e. stable end states, black dots correspond to $\text{Im}E_e > 0$, i.e. unstable end states, blue dots to $\text{Im}E_b$, i.e. bulk states. (a) $G_+ = 0.05$, (b) $G_+ = 0.242$, $\gamma = 10^{-4}$, $\gamma_{\text{end}} = 10^{-2}$ (all energies expressed in units of κ).

VIII. THIRD QUANTIZATION APPROACH

A. Hamiltonian

The real-space Hamiltonian has a form of:

$$\mathcal{H} = \sum_i \left(\vec{d}_i^\dagger \hat{P} \vec{d}_i + \vec{d}_i^\dagger \hat{Q} \vec{d}_i + \vec{d}_i^\dagger \hat{Q}^* \vec{d}_i^\dagger \right) + \sum_i \left(\vec{d}_i^\dagger \hat{R} \vec{d}_{i+1} + \vec{d}_{i+1}^\dagger \hat{R}^\dagger \vec{d}_i \right) \quad (34)$$

with \vec{d}_i describing bosonic degrees of freedom within unit cell i as a vector:

$$\vec{d}_i = \left(a_{1,i} \ b_{1,i} \ a_{2,i} \ b_{2,i} \ a_{3,i} \ b_{3,i} \ a_{4,i} \ b_{4,i} \right) \quad (35)$$

with matrices \hat{P} , \hat{Q} and \hat{R} describing hopping and pairing of the bosons inside and between unit cells. We have:

$$\hat{P} = \begin{pmatrix} 0 & 0 & 0 & 0 & 0 & 0 & 0 & 0 \\ 0 & 0 & 0 & -1 & 0 & 0 & 0 & 0 \\ 0 & 0 & 0 & G_- & 0 & 0 & 0 & 0 \\ 0 & -1 & G_- & 0 & 0 & -1 & 0 & 0 \\ 0 & 0 & 0 & 0 & 0 & G_- & 0 & 0 \\ 0 & 0 & 0 & -1 & G_- & 0 & 0 & -1 \\ 0 & 0 & 0 & 0 & 0 & 0 & 0 & 0 \\ 0 & 0 & 0 & 0 & 0 & -1 & 0 & 0 \end{pmatrix}, \quad \hat{Q} = \begin{pmatrix} 0 & G_+ & 0 & 0 & 0 & 0 & 0 & 0 \\ G_+ & 0 & 0 & 0 & 0 & 0 & 0 & 0 \\ 0 & 0 & 0 & 0 & 0 & 0 & 0 & 0 \\ 0 & 0 & 0 & 0 & 0 & 0 & 0 & 0 \\ 0 & 0 & 0 & 0 & 0 & 0 & 0 & 0 \\ 0 & 0 & 0 & 0 & 0 & 0 & 0 & 0 \\ 0 & 0 & 0 & 0 & 0 & 0 & G_+ & 0 \\ 0 & 0 & 0 & 0 & 0 & 0 & G_+ & 0 \end{pmatrix}, \quad \hat{R} = \begin{pmatrix} 0 & 0 & 0 & 0 & 0 & 0 & 0 & 0 \\ 0 & 0 & 0 & 0 & 0 & 0 & 0 & 0 \\ 0 & 0 & 0 & 0 & 0 & 0 & 0 & 0 \\ 0 & 0 & 0 & 0 & 0 & 0 & 0 & 0 \\ 0 & 0 & 0 & 0 & 0 & 0 & 0 & 0 \\ 0 & 0 & 0 & 0 & 0 & 0 & 0 & 0 \\ 0 & 0 & 0 & 0 & 0 & 0 & 0 & 0 \\ 0 & -1 & 0 & 0 & 0 & 0 & 0 & 0 \end{pmatrix}. \quad (36)$$

For a system consisting of N unit cells we can set we define a composite vector:

$$\vec{d} = (\vec{d}_1 \ \vec{d}_2 \ \dots \ \vec{d}_N) \quad (37)$$

and the Hamiltonian becomes:

$$\begin{aligned} \mathcal{H} &= \vec{d}^\dagger \left(\hat{T}_0 \otimes \hat{P} + \hat{T}_1 \otimes \hat{R} + \hat{T}_{-1} \otimes \hat{R}^\dagger \right) \vec{d} + \vec{d} \left(\hat{T}_0 \otimes \hat{Q} \right) \vec{d} + \vec{d}^\dagger \left(\hat{T}_0 \otimes \hat{Q}^* \right) \vec{d}^\dagger \\ &= \vec{d}^\dagger \hat{H} \vec{d} + \vec{d} \hat{K} \vec{d} + \vec{d}^\dagger \hat{K}^* \vec{d}^\dagger \end{aligned} \quad (38)$$

with \hat{T}_0 being $N \times N$ identity matrix and \hat{T}_1 being a matrix describing shift by one of all unit cells, i.e.,

$$\hat{T}_1 = \begin{pmatrix} 0 & 1 & & & & & & \\ & 0 & 1 & & & & & \\ & & & \ddots & & & & \\ & & & & \ddots & & & \\ & & & & & 0 & 1 & \\ x & & & & & & & 0 \end{pmatrix}, \quad \hat{T}_{-1} := \hat{T}_1^T. \quad (39)$$

Here $x = 1$ for periodic and $x = 0$ for open boundary conditions.

B. Liouvillian

Following the third quantization procedure by Prosen and Seligman [7, 14] we find that the Liouvillian can be written in the form of

$$\mathcal{L} = -2 \left(\vec{d}'_0 \ \vec{d}'_1 \right) \hat{X}^T \left(\vec{d}_0 \ \vec{d}_1 \right) + \left(\vec{d}'_0 \ \vec{d}'_1 \right) \hat{Y} \left(\vec{d}_0 \ \vec{d}_1 \right) \quad (40)$$

with operators $d_{i,\mu}$ satisfying almost canonical commutation relations for bosons:

$$[d_{i,\mu}, d'_{j,\nu}] = \delta_{ij} \delta_{\mu\nu} \quad (41)$$

where $d'_{j,\nu}$ is not Hermitian conjugate of $d_{j,\nu}$. In the Liouvillian the matrices defining Hamiltonian enter as blocks of \hat{X} and \hat{Y} :

$$\hat{X} = \frac{1}{2} \begin{pmatrix} i\hat{H}^* + \hat{M} & -2i\hat{K} \\ 2i\hat{K}^* & -i\hat{H} + \hat{M}^* \end{pmatrix}, \quad \hat{Y} = \begin{pmatrix} -i\hat{K}^* & 0 \\ 0 & i\hat{K} \end{pmatrix}, \quad (42)$$

where \hat{M} is matrix describing dissipation. In our case it takes a diagonal form of:

$$\hat{M} = \hat{T}_0 \otimes \frac{1}{2} \text{diag} \left(\kappa \ \gamma \ \kappa \ \gamma \ \kappa \ \gamma \ \kappa \ \gamma \right). \quad (43)$$

Liouvillian is a quadratic form of boson-like operators and can be brought to a diagonal form of

$$\mathcal{L} = -2 \sum_{i=1}^{16N} \beta_i \xi'_i \xi_i, \quad (44)$$

by a suitable symplectic transformation. One finds that the rapidities β_i are the eigenvalues of the matrix \hat{X} so that one can identify X to be proportional to the non-Hermitian Hamiltonian of the system. Strictly speaking we can identify:

$$\hat{H}_{\text{NH}} = -2i\hat{X}. \quad (45)$$

C. Time-evolution

To maximally simplify the notation let's write the Liouvillian as

$$\mathcal{L} = \bar{\alpha}' \hat{A} \bar{\alpha} + \bar{\alpha}' \hat{B} \bar{\alpha}', \quad (46)$$

with a_i and a'_i being almost canonical bosons and \hat{A} , \hat{B} being $L \times L$ matrices. Now, the third-quantized Lindblad equation reads:

$$\frac{d}{dt} \rho(t) = \mathcal{L}[\rho] \quad (47)$$

thus the time-evolution of the density matrix is given by

$$|\rho(t)\rangle = \exp[t\mathcal{L}] |\rho(0)\rangle. \quad (48)$$

The solution has a form of

$$|\rho(t)\rangle = \mathcal{T} \exp \left[\int_0^t dt' \mathcal{L}(t') \right] \rho(0). \quad (49)$$

Taking a coherent state as initial

$$|\rho(0)\rangle = |\bar{z}(0)\rangle = \exp[\bar{z}(0)\bar{\alpha}'] |0\rangle, \quad (50)$$

using Suzuki-Trotter decomposition and resolution of identity in coherent states we get:

$$|\rho(t)\rangle = \frac{1}{\pi^{2LN_t}} \int \left(\prod_{i=1}^{N_t} d\Im \bar{z}_i d\Re \bar{z}_i \right) \exp \left[\sum_{i=1}^{N_t} S_i \right] |\bar{z}_1\rangle, \quad (51)$$

with

$$S_i = \bar{z}_i^* \left[1 + \frac{t}{N_t} \hat{A} \right] \bar{z}_{i+1} + \bar{z}_i^* \left[\frac{t}{N_t} \hat{B} \right] \bar{z}_i - \bar{z}_i^* \bar{z}_i \quad (52)$$

and $\bar{z}_{N_t+1} \equiv \bar{z}(0)$ for number of time-steps $N_t \rightarrow \infty$. By calculating multi-dimensional Gaussian integral we can get:

$$|\rho(t)\rangle = \frac{1}{\pi^{2L}} \int d\Im \bar{z} d\Re \bar{z} \exp \left[-\bar{z}^* \bar{z} + \bar{z}^* \exp \left[t\hat{A} \right] \bar{z}(0) + \frac{t}{N_t} \bar{z}^* \left[\hat{B} + \hat{h}\hat{B}\hat{h}^T + \dots + \hat{h}^{N-1}\hat{B}(\hat{h}^T)^{N-1} \right] \bar{z} \right] |\bar{z}\rangle. \quad (53)$$

with

$$\hat{h} = 1 + \frac{t}{N} \hat{A}. \quad (54)$$

The series in the exponent can be summed up in a similar way one is summing up a finite geometric series. Then we get for $N_t \rightarrow \infty$:

$$|\rho(t)\rangle = \frac{1}{\pi^{2L}} \int d\Im \bar{z} d\Re \bar{z} \exp \left[-\bar{z}^* \bar{z} + \bar{z}^* \exp \left[t\hat{A} \right] \bar{z}(0) + \bar{z}^* \hat{C}(t) \bar{z} \right] |\bar{z}\rangle \quad (55)$$

with $\hat{C}(t)$ being a matrix that satisfy Lyapunov equation of the form

$$\hat{A}\hat{C}(t) + \hat{C}(t)\hat{A}^T = \exp \left[t\hat{A} \right] \hat{B} \exp \left[t\hat{A}^T \right] - \hat{B}. \quad (56)$$

After performing final Gaussian integration the time-evolved density matrix becomes:

$$|\rho(t)\rangle = \exp \left[\bar{\alpha}' \hat{C}(t) \bar{\alpha}' \right] \left| \exp \left[t\hat{A} \right] \bar{z}(0) \right\rangle. \quad (57)$$

D. Solution of the Lyapunov equation

The Lyapunov equation is known to have a solution of the closed form:

$$\hat{C}(t) = \int_0^t \exp[x\hat{A}] \hat{B} \exp[x\hat{A}^T] dx. \quad (58)$$

Assuming that \hat{A} can be diagonalized in the eigenbasis $\hat{\beta}$ we get:

$$\hat{\Lambda} = \hat{\beta}^{-1} \hat{A} \hat{\beta} = \text{diag}(\lambda_1 \ \lambda_2 \ \dots \ \lambda_{2L}) = \hat{\beta}^T \hat{A}^T \hat{\beta}^{-1T}. \quad (59)$$

Thus:

$$\hat{\beta}^{-1} \hat{C}(t) \hat{\beta}^{-1T} = \int_0^t \exp[x\hat{\Lambda}] \hat{\beta}^{-1} \hat{B} \hat{\beta}^{-1T} \exp[x\hat{\Lambda}] dx \quad (60)$$

or:

$$\begin{aligned} \left(\hat{\beta}^{-1} \hat{C}(t) \hat{\beta}^{-1T} \right)_{ij} &= \left(\hat{\beta}^{-1} \hat{B} \hat{\beta}^{-1T} \right)_{ij} \\ &\times \int_0^t dx \exp[x(\lambda_i + \lambda_j)]. \end{aligned} \quad (61)$$

Then by explicitly calculating the integral we finally get:

$$\hat{C}(t) = \hat{\beta} \left[\left(\hat{\beta}^{-1} \hat{B} \hat{\beta}^{-1T} \right) \circ \hat{\Gamma}(t) \right] \hat{\beta}^T, \quad (62)$$

with

$$\Gamma_{ij}(t) = \frac{\exp[t(\lambda_i + \lambda_j)] - 1}{\lambda_i + \lambda_j} \quad (63)$$

and \circ denoting Hadamard product of matrices.

E. Correlation functions

After starting from the Liouvillian of the general third-quantized form of Eq. (46) and getting the time-evolved density matrix $|\rho(t)\rangle$ in the form of Eq. (57) we can easily compute single or multi-boson correlation functions. First, we need to make contact with our model Liouvillian of Eq. (40). We have:

$$\vec{\alpha} = \left(\vec{d}_0 \ \vec{d}_1 \right), \quad \hat{A} = -2\hat{X}^T, \quad \hat{B} = \hat{Y}. \quad (64)$$

Here the 'flavor' index $\mu = 0, 1$ of \vec{d}_μ is an effect of third quantization whereas all other indices of \vec{d} describe physical bosonic modes of the system. Therefore it makes sense to define a subblock structure of matrices \hat{A} , \hat{B} and $\hat{C}(t)$, i.e.:

$$\hat{A} = \begin{pmatrix} \hat{A}^{00} & \hat{A}^{01} \\ \hat{A}^{01} & \hat{A}^{11} \end{pmatrix}, \quad \hat{B} = \begin{pmatrix} \hat{B}^{00} & \hat{B}^{01} \\ \hat{B}^{01} & \hat{B}^{11} \end{pmatrix}, \quad \hat{C} = \begin{pmatrix} \hat{C}^{00} & \hat{C}^{01} \\ \hat{C}^{01} & \hat{C}^{11} \end{pmatrix}. \quad (65)$$

Now we can calculate some correlation function. Start with creator-annihilator average. Following third quantization we get:

$$\text{Tr} \left(d_i^\dagger d_j \rho(t) \right) = \langle 0 | (d'_{i,0} + d_{i,1}) d_{j,0} | \rho(t) \rangle = \langle 0 | d_{i,1} d_{j,0} | \rho(t) \rangle. \quad (66)$$

The last expression can be easily calculate from the integral form of the density matrix $|\rho(t)\rangle$ of Eq. (55), namely:

$$\text{Tr} \left(d_i^\dagger d_j \rho(t) \right) = \frac{1}{\pi^{2L}} \int d\Im z d\Re z \ z_{i,1} z_{j,0} \times \exp \left[-z^* z + z^* \exp[t\hat{A}] z(0) + z^* \hat{C}(t) z^* \right]. \quad (67)$$

From the Gaussian integral we get:

$$\text{Tr} \left(d_i^\dagger d_j \rho(t) \right) = C(t)_{ij}^{10} + C(t)_{ji}^{01} + \left(\exp \left[t \hat{A} \right] \bar{z}(0) \right)_{i,1} \left(\exp \left[t \hat{A} \right] \bar{z}(0) \right)_{j,0}. \quad (68)$$

In analogical way we can get other single-boson correlators, i.e.,

$$\text{Tr} \left(d_i^\dagger d_j^\dagger \rho(t) \right) = C(t)_{ij}^{11} + C(t)_{ji}^{11} + \left(\exp \left[t \hat{A} \right] \bar{z}(0) \right)_{i,1} \left(\exp \left[t \hat{A} \right] \bar{z}(0) \right)_{j,1} \quad (69)$$

and

$$\text{Tr} \left(d_i d_j \rho(t) \right) = C(t)_{ij}^{00} + C(t)_{ji}^{00} + \left(\exp \left[t \hat{A} \right] \bar{z}(0) \right)_{i,0} \left(\exp \left[t \hat{A} \right] \bar{z}(0) \right)_{j,0}. \quad (70)$$

If the starting state is not vacuum but a generic coherent state then also the linear averages of creation/annihilation operators are non-trivial. We get:

$$\text{Tr} \left(d_i^\dagger \rho(t) \right) = \left(\exp \left[t \hat{A} \right] \bar{z}(0) \right)_{i,1}, \quad (71)$$

$$\text{Tr} \left(d_i \rho(t) \right) = \left(\exp \left[t \hat{A} \right] \bar{z}(0) \right)_{i,0}. \quad (72)$$

F. Non-zero temperature

In presence of non-zero temperature the Liouvillian of Eq. (40) gets modified by new form of the \hat{X} and \hat{Y} matrices, one gets:

$$\hat{X} = \frac{1}{2} \begin{pmatrix} i\hat{H}^* + \hat{M} - \hat{N}^* & -2i\hat{K} \\ 2i\hat{K}^* & -i\hat{H} + \hat{M}^* - \hat{N} \end{pmatrix}, \quad \hat{Y} = \begin{pmatrix} -i\hat{K}^* & \hat{N} \\ \hat{N}^* & i\hat{K} \end{pmatrix}, \quad (73)$$

where the definitions of the \hat{M} and \hat{N} block are given by:

$$\hat{N} = \hat{T}_0 \otimes \frac{1}{2} \text{diag} \left(\kappa n_a \quad \gamma n_b \quad \kappa n_a \quad \gamma n_b \quad \kappa n_a \quad \gamma n_b \quad \kappa n_a \quad \gamma n_b \right), \quad (74)$$

$$\hat{M} = \hat{T}_0 \otimes \frac{1}{2} \text{diag} \left(\kappa(n_a + 1) \quad \gamma(n_b + 1) \quad \kappa(n_a + 1) \quad \gamma(n_b + 1) \quad \kappa(n_a + 1) \quad \gamma(n_b + 1) \quad \kappa(n_a + 1) \quad \gamma(n_b + 1) \right). \quad (75)$$

Here n_a and n_b are thermal occupations of the a and b bosonic modes, so for zero temperature $\hat{N} = 0$ and the \hat{X} and \hat{Y} matrices take the old form of Eq. (42). With new form of the Liouvillian the rest of derivation is done in the same manner.

G. Stationary correlation matrix

Using equations (68-70) it is simple to relate matrix \hat{C} with the correlation matrix \hat{V} . First one has to notice that from the solution of the Lyapunov equation it follows that \hat{C} is symmetric. Therefore taking initial condition as vacuum, i.e., $\bar{z}(0) = 0$ we get for stationary state averages:

$$\begin{aligned} C_{ij}^{00} &= \langle d_i d_j \rangle / 2 \\ C_{ij}^{11} &= \langle d_i^\dagger d_j^\dagger \rangle / 2 = C_{ij}^{00*} \\ C_{ij}^{10} &= \langle d_i^\dagger d_j \rangle / 2 \\ C_{ij}^{01} &= \langle d_i d_j^\dagger - \delta_{ij} \rangle / 2 = \langle a_j^\dagger a_i \rangle / 2 = C_{ji}^{10} \end{aligned} \quad (76)$$

The correlation matrix can be written blockwise as:

$$\hat{V} = \begin{pmatrix} \hat{V}^{00} & \hat{V}^{01} \\ \hat{V}^{10} & \hat{V}^{11} \end{pmatrix} \quad (77)$$

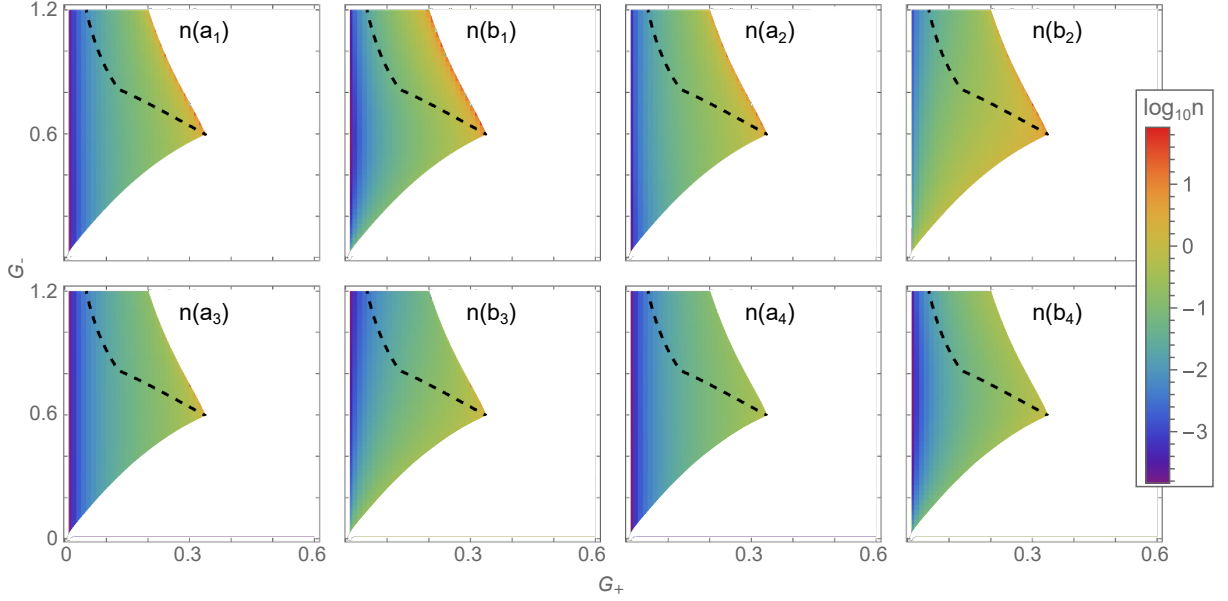


Figure 7. Stationary-state densities for $\gamma = 0.0001$ and $\kappa = 1.0$. Dashed line indicates boundary of end-states hidden in the bulk. Densities diverge in the white excluded region as there is no stationary state.

with blocks given by elements: $V_{ij}^{00} = \langle d_i d_j^\dagger \rangle$, $V_{ij}^{01} = \langle d_i d_j \rangle$, $V_{ij}^{10} = \langle d_i^\dagger d_j^\dagger \rangle$ and $V_{ij}^{11} = \langle d_i^\dagger d_j \rangle$. Thus \hat{C} matrix can be written as:

$$\hat{C} = \frac{1}{2} \begin{pmatrix} \hat{V}^{01} & \hat{V}^{00} - 1 \\ \hat{V}^{11} & \hat{V}^{10} \end{pmatrix} = \frac{1}{2} \left[\begin{pmatrix} \hat{V}^{00} & \hat{V}^{01} \\ \hat{V}^{10} & \hat{V}^{11} \end{pmatrix} - \begin{pmatrix} 1 & 0 \\ 0 & 0 \end{pmatrix} \right] \begin{pmatrix} 0 & 1 \\ 1 & 0 \end{pmatrix}. \quad (78)$$

Now we can insert such form of matrix \hat{C} into the stationary-state Lyapunov equation:

$$\hat{A}\hat{C} + \hat{C}\hat{A}^T = -\hat{B} \quad (79)$$

we get an equation for the \hat{V} matrix:

$$\begin{pmatrix} 2\hat{M} & 0 \\ 0 & 2\hat{N} \end{pmatrix} = \begin{bmatrix} i \begin{pmatrix} \hat{H} - i(\hat{M} - \hat{N}) & 2\hat{K} \\ -2\hat{K} & -\hat{H} - i(\hat{M} - \hat{N}) \end{pmatrix} \\ + \begin{pmatrix} \hat{V}^{00} & \hat{V}^{01} \\ \hat{V}^{10} & \hat{V}^{11} \end{pmatrix} \begin{bmatrix} i \begin{pmatrix} \hat{H} - i(\hat{M} - \hat{N}) & 2\hat{K} \\ -2\hat{K} & -\hat{H} - i(\hat{M} - \hat{N}) \end{pmatrix} \end{bmatrix}^\dagger \end{bmatrix}, \quad (80)$$

or simply:

$$(i\hat{H}_{\text{NH}})\hat{V} + \hat{V}(i\hat{H}_{\text{NH}})^\dagger = \begin{pmatrix} 2\hat{M} & 0 \\ 0 & 2\hat{N} \end{pmatrix}. \quad (81)$$

For this derivation we have taken advantage of the present current form of the Hamiltonian with $\hat{H} = \hat{H}^T$, $\hat{K} = \hat{K}^T = \hat{K}^*$. Note that the non-Hermitian Hamiltonian \hat{H}_{NH} does not depend on temperature.

H. Entanglement in the presence of unstable end modes

Surprisingly, the entanglement can be calculated also when there is no stationary state because the end modes are unstable. In this case there are four degenerate end-modes which become unstable so the $\hat{C}(t)$ matrix can be

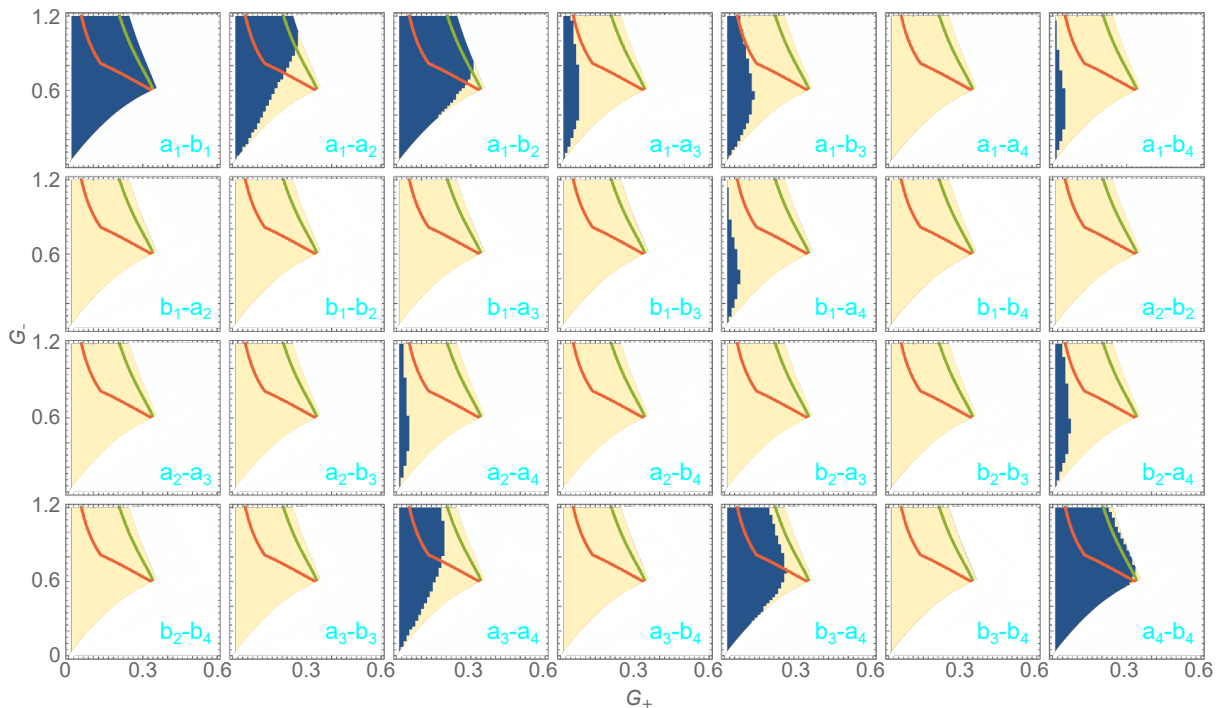


Figure 8. Entanglement patterns for $\gamma = 0.0001$ and $\kappa = 1.0$. Dark/bright color indicates non-vanishing/vanishing stationary state- or saturation-negativity between two modes denoted in cyan in bottom right corner of each panel. Red and green lines indicates boundaries of: end-states hidden in the bulk and end of the system having stationary state. In the excluded white region the bulk has no stationary state. In the region between green line and white area the populations are diverging due to the instability of the end-states but negativity remains finite.

evaluated from Eq. (62) in the limit of $t \rightarrow \infty$ by setting:

$$\Gamma_{ij}(t \rightarrow \infty) \rightarrow \frac{1}{\lambda_i + \lambda_j} \left[\begin{pmatrix} -1 & \cdots & -1 \\ \vdots & \ddots & \vdots \\ -1 & \cdots & -1 \end{pmatrix} \oplus \begin{pmatrix} \xi & \xi & \xi & \xi \\ \xi & \xi & \xi & \xi \\ \xi & \xi & \xi & \xi \\ \xi & \xi & \xi & \xi \end{pmatrix} \right]_{ij} \quad (82)$$

with $\xi = \exp[2t\lambda_{\text{end}}]$. Clearly ξ diverges when $t \rightarrow \infty$. Using this form of $\hat{\Gamma}$ matrix and keeping ξ as analytical variable we can express $\hat{C}(\xi \rightarrow \infty)$ and any two-point correlation function as analytical expression in ξ . Then we can quantify the entanglement for $t \rightarrow \infty$ by computing $\tilde{\nu}_-$ and taking analytical limit of $\tilde{\nu}_-(\xi \rightarrow \infty)$. Quite non-trivially this limit is well-defined and finite despite diverging populations of bosons.

IX. ENTANGLEMENT MEASUREMENT

We sketch here a possible detection scheme for the optomechanical entanglement within the end sites of the chain. Following a known strategy [15], we suggest that the inclusion of an extra cavity coupled to the mechanical resonators at each end of the chain can be employed to monitor the mechanical motion of the extremal sites of the superlattice. To this end, each detection cavity is weakly driven on the red sideband, inducing an effective beam-splitter interaction between mechanical (b_1, b_{4N}) and readout (c, d) degrees of freedom (see Fig. 9).

In the following we focus, without loss of generality on the first site of the chain. The detection cavity described by bosonic operators c and c^\dagger , is weakly driven on the red sideband, giving rise (in the appropriate frame) to the following EOM for c in Fourier space

$$-i\omega c = \frac{\kappa}{2}c - iG_R b_1 + \sqrt{\kappa}c \quad (83)$$

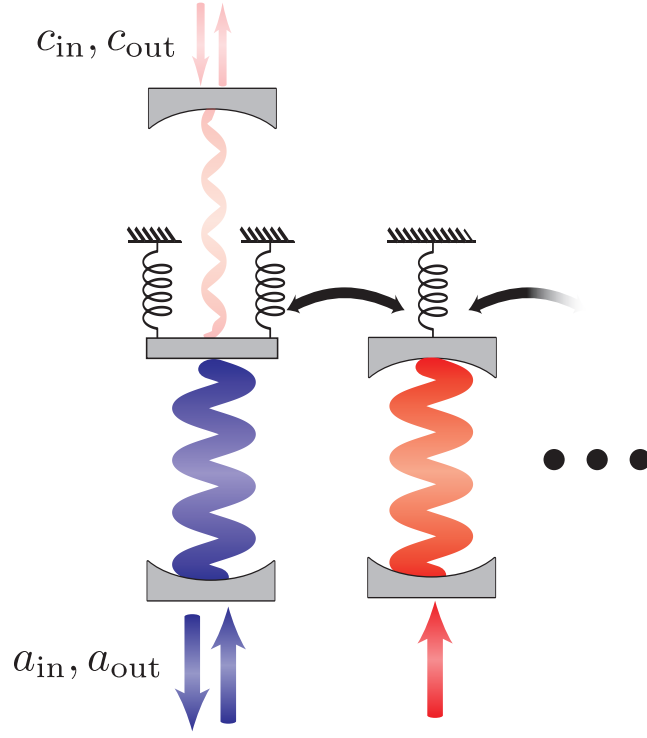


Figure 9. Cartoon depiction of the left end in the presence of an extra detection cavity weakly driven on the red sideband (intracavity mode c , input/output modes $c_{\text{in}}, c_{\text{out}}$).

where, G_{R} and κ_{R} are the coupling induced by the detection drive and the detection cavity linewidth, respectively. Hereafter, we will assume $\kappa_{\text{R}} = \kappa$. Taking into account the usual input-output relations

$$c_{\text{out}} = \sqrt{\kappa} c - c_{\text{in}} \quad (84\text{a})$$

$$a_{\text{out}} = \sqrt{\kappa} a - a_{\text{in}} \quad (84\text{b})$$

[16], the output field for the readout cavity can be written as

$$c_{\text{out}} = (\chi_c \kappa - 1) c_{\text{in}} - i \chi_c G_{\text{R}} \sqrt{\kappa} b_1. \quad (85)$$

If we assume that the detection tone G_{R} is much weaker than the driving tone G_+ , the dynamics of the optomechanical system is essentially unchanged by the detection process, simply leading to the renormalization of γ and n_{eff} . As far as the superlattice is concerned, we have demonstrated that our protocol is robust with respect to changes in the thermal population and, in Section VIIC of the SI, we have numerically demonstrated the fact that, owing to the topological features of our system, enlargement is robust also for large variations of the mechanical linewidth on the end sites.

Assuming that the cavities are coupled to a zero-temperature bath, we can relate the (normal-ordered) power spectrum of the correlations between the output fields

$$S_{1,2}^{\text{out}}(\omega) = \int \frac{d\omega'}{2\pi} \langle O_{1,\text{out}}^\dagger(\omega) O_{2,\text{out}}(\omega') \rangle \quad (86)$$

(where $O_{1,\text{out}}, O_{2,\text{out}} = a_{\text{out}}, c_{\text{out}}$) to the power spectrum of the correlations between a and c (and, consequently, b) [9, 16], given that

$$S_{1,2}^{\text{out}}(\omega) = \kappa S_{1,2}(\omega). \quad (87)$$

-
- [1] A. H. Safavi-Naeini and O. Painter, Design of optomechanical cavities and waveguides on a simultaneous bandgap phononic-photonic crystal slab, *Optics Express* **18**, 14926 (2010).
 - [2] O. Painter, R. K. Lee, A. Scherer, A. Yariv, J. D. O'Brien, P. D. Dapkus, and I. Kim, Two-Dimensional Photonic Band-Gap Defect Mode Laser, *Science* **284**, 1819 (1999).
 - [3] J. Vučković, M. Lončar, H. Mabuchi, and A. Scherer, Design of photonic crystal microcavities for cavity QED, *Physical Review E* **65**, 016608 (2002).
 - [4] J. O. Vasseur, A.-C. Hladky-Hennion, B. Djafari-Rouhani, F. Duval, B. Dubus, Y. Pennec, and P. A. Deymier, Waveguiding in two-dimensional piezoelectric phononic crystal plates, *Journal of Applied Physics* **101**, 114904 (2007).
 - [5] R. H. O. III and I. El-Kady, Microfabricated phononic crystal devices and applications, *Measurement Science and Technology* **20**, 012002 (2009).
 - [6] M. Ludwig and F. Marquardt, Quantum Many-Body Dynamics in Optomechanical Arrays, *Physical Review Letters* **111**, 073603 (2013).
 - [7] W. Brzezicki, M. Silveri, M. Płodzień, F. Massel, and T. Hyart, Non-Hermitian topological quantum states in a reservoir-engineered transmon chain, *Physical Review B* **107**, 115146 (2023).
 - [8] M. Aspelmeyer, T. J. Kippenberg, and F. Marquardt, Cavity optomechanics, *Reviews of Modern Physics* **86**, 1391 (2014).
 - [9] C. W. Gardiner and P. Zoller, *Quantum noise*, Springer (Springer, 2004).
 - [10] C. W. Gardiner, *Handbook of Stochastic Methods for Physics, Chemistry and the Natural Sciences*, Springer Series in Synergetics (Springer series in synergetics, 2004).
 - [11] G. Adesso and F. Illuminati, Entanglement in continuous-variable systems: recent advances and current perspectives, *Journal of Physics A: Mathematical and Theoretical* **40**, 7821 (2007).
 - [12] W. Brzezicki and T. Hyart, Hidden Chern number in one-dimensional non-Hermitian chiral-symmetric systems, *Physical Review B* **100**, 161105 (2019).
 - [13] A. Youssefi, S. Kono, A. Bancora, M. Chegnizadeh, J. Pan, T. Vovk, and T. J. Kippenberg, Topological lattices realized in superconducting circuit optomechanics, *Nature* **612**, 666 (2022).
 - [14] T. Prosen and T. H. Seligman, Quantization over boson operator spaces, *Journal of Physics A: Mathematical and Theoretical* **43**, 392004 (2010).
 - [15] D. Vitali, S. Gigan, A. Ferreira, H. R. Böhm, P. Tombesi, A. Guerreiro, V. Vedral, A. Zeilinger, and M. Aspelmeyer, Optomechanical Entanglement between a Movable Mirror and a Cavity Field, *Physical Review Letters* **98**, 030405 (2007).
 - [16] D. F. Walls and G. J. Milburn, *Quantum Optics*, Quantum Optics (Springer Berlin Heidelberg, 2008).